Department of Physics
University College London

# Preparatory work for $C_3$ line-list calculation

*Author:*
Santina La Delfa

*Supervisor:*
Prof. J. Tennyson

Thesis Submitted for M.Phil.

May 15, 2008

## 0.1 Abstract

The goal of this dissertation is to study the infrared absorption spectrum of the $C_3$ (carbon three) molecule. In particular, the aim is to investigate its ground electronic state up to 12.500 $cm^{-1}$, as this affects the atmospheres of cool C-rich stars.

The linear $C_3$ molecule shows very unusual properties for a linear molecule: a high degree of floppiness, no permanent dipole moment and a strong bent-stretch interaction. Consequently, the $C_3$ spectrum presents particular features such as as overtones, hot bands, and, as has been recently detected in Carbon stars and molecular clouds, a quite low fundamental bending frequency (63 $cm^{-1}$) when in the ground electronic state. This dissertation aims to address each of these features.

The first section discusses the context for this work: the stars. It provides a brief introduction about the Astrophysics related to this research project. A review at the recent literature is provided and the experimental results which provide the goal for the results of the theoretical work in the rest of the dissertation are set out.

The second section introduces the $C_3$ molecule and outlines its properties. Previous $C_3$ studies are discussed and the theoretical approach used to study ro-vibrational spectra of triatomic molecules is set out. Preparatory tests and calculations are carried out to allow a theoretical reproduction of $C_3$ rotovibrational spectrum in the infrared region to be produced.

The third part of the thesis expands on the nuclear motion calculations of section 2 and presents the results of the large scale calculations performed using the DVR3D suit programs written by Tennyson *et al.* [1]. This program allows the calculation of energy levels, wave-functions, expectation values and Einstein Coefficients. It takes as input the Potential Energy Surface (PES) and a Dipole Moment Surface (DMS) constructed a priori (in section 2) by solving the electronic problem within the Born-Oppenheimer's approximation.

Because the quality of the PES sets the accuracy of the ro-vibrational calculations tests on different $C_3$ PESs and DMSs are performed. To reproduce accurate spectra of cool stars atmosphere in the temperature range of

$2000 - 4000\ K$ it was necessary perform calculations with high rotational quantum number. For this reason, tests with $J \gg 0$ were necessary to optimize the DVR3DRJZ parameters in order to guarantee a certain degree of accuracy and energy levels convergence.

The results of these calculations and associated $C_3$ line-lists should be very useful to support to the observations and model atmospheric studies.

This work was generously supported by the QUASAAR Marie Curie Network.

# Contents

# Chapter 1

# Modelling the Opacity of Cool Stars

The number of molecular species observed in space is about 140 and their formation is determined by the surronding environment. Many of these species are found in stars. Stars tehrefore, and in particular Carbon stars are the main target of this study.

In this section we discuss the properties of the astrophysical environments. Our overall aim is to look at properties that will effect results from spectroscopy. Spectroscopy is the technique of analysing light coming from space to determine the properties of a remote object. Depending on the physical conditions of the particular environment under investigation, matter presents different structure, phase and composition.

We first introduce the method of spectroscopy before looking at the stellar parameters that effect it. The main ones will be brightness, radiation transfer and opacity effects. Finally we will give a brief explanation of stellar evolution and how the stellar parameters determine where in the evolutionary sequence a star is.

## 1.1 Molecular Spectroscopy

Molecular Spectroscopy is a technique for investigating the microscopic properties of molecules. Nowadays it is known to be the most powerful tool for finding detailed microscopic information about molecular systems. As such, many experiments and computational chemical investigations using this technique have been completed in the past few years.

A molecule is made up of a number of atoms, these may be positive or negatively charged. The distribution of these charges create what is known as a dipole moment; a measure of the strength of charge and geometry of the molecule.

The basic principle behind Molecular Spectroscopy is that infra-red radiation (the electromagnetic spectrum between 0.78 and 1000mm) is energetic enough to stimulate vibrations or rotations within a molecule. The alternating electrical field of the infra-red radiation interacts with fluctuations in the dipole moment of a given molecule. When the radiation matches the vibrational frequency of the molecule, radiation will be absorbed. This means that at this frequency there will be a reduced intensity of infra-red radiation. Each molecule therefore gives a characteristic 'fingerprint' with varying intensities of radiation at different frequencies.

Every molecule possesses a unique spectrum or 'fingerprint'. This means that by looking at a series of 'fingerprints' from a remote environment (a star for example) the molecular make up of that environment can be determined. This means that qualitative and quantitative information about observed astrophysical objects such as planets, stars, interstellar medium, nebulae and so on can be determined.

In astrophysics, spectroscopy therefore sometimes represents the only 'way of knowledge'. For this reason it is really important know a-priori the features of a molecule to be able to identify it through spectra.

## 1.2 Stellar Parameters

### 1.2.1 Brightness

As you can see on a clear night – stars shine and some are more bright than others. In order to quantify this idea of brightness we consider the amount of energy emitted by a star that reaches us – the observer.

The amount of radiation at a given frequency $\nu$ from a star passing any given surface is known as the energy flux of the star $F_\nu$. The energy flux is the amount of radiation $E$ passing through one square centimeter of a surface in one second multiplied by the surface area $S$ for one unit of frequency *i.e.*

$$F_\nu = \frac{\mathrm{d}E}{\mathrm{d}\nu\,\mathrm{d}t\,\mathrm{d}S}. \tag{1.2.1}$$

Say a star has a certain luminous power at a given frequency $\nu$ (which we call Luminosity $L_\nu$). If we imagine a sphere of radius $d$ centered on the star then all the energy emitted by the star must pass through the surface of the sphere. The total energy flux $F_\nu$ passing through the sphere must be the luminosity averaged over the surface area of the sphere ($4\pi d^2$) so

$$L_\nu = 4\pi d^2 F_\nu. \tag{1.2.2}$$

The star is not just a point at the centre of the sphere we imagined above but rather it is itself a (approximate) sphere radius $r$ – a sphere within a sphere. The observed brighness of a star will need to be adjusted for by its size. The solid angle under which a star is observed, $\Delta\Omega$, is a measure of how big that object appears to an observer looking from that point. We therefore define the intensity (or brilliance) of radiation $I_\nu$ as the power radiated in a certain direction by:

$$I_\nu = \frac{F_\nu}{\Delta\Omega}, \tag{1.2.3}$$

We note that distance of the star from the observer, $d$, is much greater than its radius, $r$, ($d$ has order of magnitude $10^{13}$m where as $r$ is more like $10^7$m), therefore the flux $F_{\nu,S}$ can be considered as emitted from a point source:

$$F_\nu = F_{\nu,S}S = F_{\nu,S}(\frac{r^2}{d}), \tag{1.2.4}$$

$$\tag{1.2.5}$$

The solid angle subtended by the surface S has formula:

$$\Delta\Omega = \frac{S}{d} = \frac{\pi r^2}{d}, \tag{1.2.6}$$

$$\tag{1.2.7}$$

$$\begin{aligned} I_\nu &= \frac{F_\nu}{\Delta\Omega}, & (1.2.8)\\ &= F_{\nu,S}(\frac{r^2}{d})/(\frac{\pi r^2}{d}) = \frac{F_{\nu,S}}{\pi}, & (1.2.9) \end{aligned}$$

So surprisingly as can be seen from equation (1.2.9), intensity is independent of the distance $d$ between the star and earth.

We now introduce the concept of an idealaised object called a black body. This is any object that has the property of absorbing any radiation that hits it and emitting the same amount of radiation it absorbs. As it neither gains nor loses energy a black body's radiation is therefore in thermodynamic equilibrium and it had a spectrum that depends only on its temperature $T$.

Experiments to reproduce and study black body radiation were performed in 19th century by Kirchoff. The radiation coming out from a small hole in the reflective walls of a hot cavity in thermodynamic equilibrium was used as sample of black body's radiation.

Light in the cavity can be thought of as waves in stationary conditions. The number of normal modes (resonant frequencies) of this oscillating system

grow exponentially with the frequency. From a classical point of view, an oscillating system presents the same probability for all modes to be produced. Howeber, it was observed that there were in fact less higer frequency modes in experiments.

Planck introduced quantum mechanics to explain the light behaviour at high frequencies where classical expression was not adequate. Using quantized modes instead, he showed that higer frequency modes are less probable then lower ones. Planck's built an expression for brilliance of a black body to explain correctly observations over the whole spectrum.

$$I_{\nu,BB} = \frac{2hc^2}{\lambda^5} \frac{1}{e^{\frac{hc}{k\lambda T}} - 1}, \tag{1.2.10}$$

where $\lambda$ is wavelength, $h$ is Planck's constant ($6.626068 \times 10^{34}\mathrm{m}^2\mathrm{kg/s}$), $k$ is Boltzmann constant ($1.3806503 \times 10^{23}\mathrm{m}^2\mathrm{kgs}^{-2}\mathrm{K}^{-1}$), $c$ is speed of light ($3 \times 10^8\mathrm{ms}^{-1}$).

It is then possible to compare the brilliance of a star to the brilliance of an idealised black body:

$$I_{\nu,STAR} = I_{\nu,BB}. \tag{1.2.11}$$

Therfore, from equation (1.2.9) the flux is given by

$$F_{\nu,S} = C \left( e^{\frac{hc}{k\lambda T}} - 1 \right)^{-1}, \tag{1.2.12}$$

where $C = 2\pi hc^2/\lambda^5$ is a constant.

From equation (1.2.12) we can calculate:

**Temperature of Brilliance** $T_\lambda$ the temperature of a black body emitting at wavelength $\lambda$ the same amount of radiation as detected from the star under investigation.

$$T_\lambda = \frac{\lambda^4}{2c} \frac{F_\lambda}{\pi}, \tag{1.2.13}$$

**Surface Temperature** $T_{Star}$ the temperature of brilliance integrated over the whole range of frequencies

$$T_{Star} = \int T_\lambda d\lambda. \tag{1.2.14}$$

**Effective Temperature** $T_{Eff}$ the temperature of a distribution of black bodies that best approximates the spectrum of the observed star.

$$T_{Eff} = \left(\frac{F}{\sigma}\right)^{\frac{1}{4}}, \tag{1.2.15}$$

where $\sigma = \dfrac{2\pi^5 k^4}{15c^2h^3}$ and $h$ is Planck's constant, $k$ is Boltzmann constant, $c$ is speed of light.

**Results of Brightness Measurements**

We have seen that from the measurement of brighness at different wavelengths it is possible to discover various properties about remote bodies. In particular we have seen that the temperature and luminosity of a remote bodies can be infered from these measurements. These two properties in turn can be used to determine which group a star belongs to.

Surface temperature and luminosity are the parameters used by Hertzsprung and Russel to classify the stars into groups: main sequence; giants branch; white dwarf sequence; and very bright but rather cool stars known as supergiants (these groups will be discussed in greated detail in Section 1.3). This sequence is known as a H-R (Hertzsprung and Russel) diagram and is shown in Figure 1.1.

### 1.2.2 Transport Models

The radiation produced by nuclear reactions in the star's core, passes through internal layers and emerges from the surface before travelling towards earth and the spectrometer we may use to look at the 'fingerprint' of the star.

Depending on the physical properties of the layers crossed, different energy transport processes may occur.

**Radiative Transport** High-energy photons are able to excite nuclei which in turn generate cooler photons. This process is called radiative transport

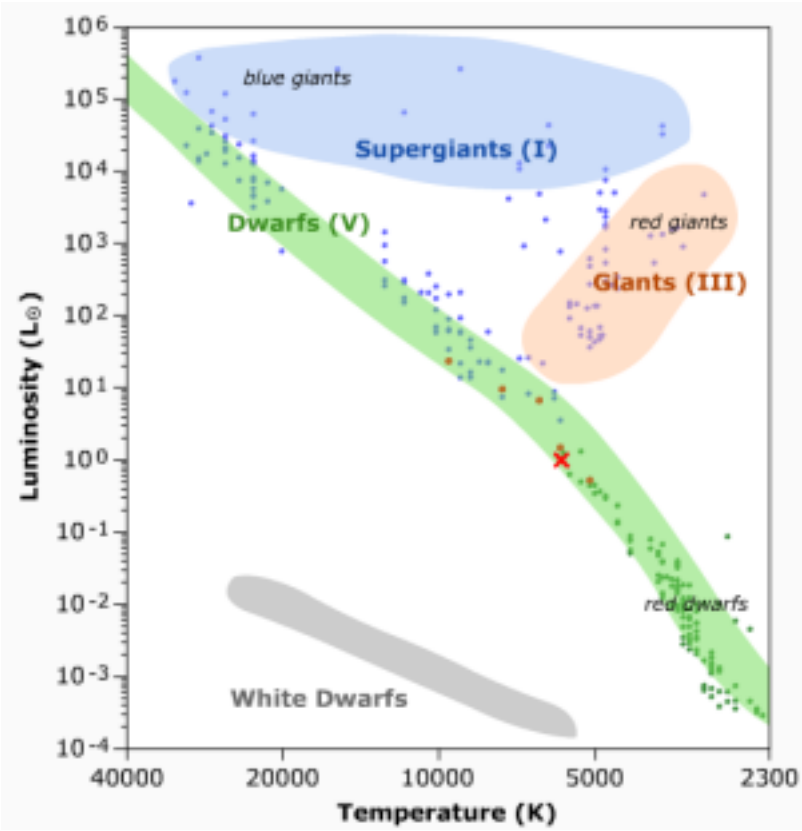


Figure 1.1: Hertzsprung and Russel Diagram

and takes place on the surface layers or near the core where high−energy photons are available.

**Condutive Transport** The heat of the core increases the kinetic energy of the material around it which will slowly diffuse towards the surface in a process known as conductive transport.

**Convective Transport** When the chaotic motion of heated material cells gains a preferential direction towards the surface, heat will be released to the cooler external layers and the cell will move back toward the centre, creating a circular motion known as convection.

As discussed at the beginning of this Section, stellar spectra are an indirect representation of stellar atmosphere chemical abundances and physical

conditions such as temperature and pressure. They are characterized by a continuum energy distribution with several absorption or emission lines (a drop or a spike in the continuum radiation at the wavelength associated).

The simplest model therefore is to ignore the dynamic transportive effects (conduction and convection) and consider only radiative transfer of energy.

However, we should be aware that spectra can show asymmetry in the line profile. Time variability and doubling effects can occur as result of coupling effects between convective motion, radiation and instability effects. In this case spectra interpretation becomes more complicated and the simple radiative transfer models excluding dynamical effects caused by convection are not reliable. In general however the models based only on radiative transfer models are often used as approximation.

### The Radiative Transport Model

The standard radiative transfer model is that based on the local thermodynamic equilibrium mentioned in the previous Section where the radiation distribution curve of a star's atmosphere can be approximated by the Black Body (or Planck's) curve. If the temperature $T$, of a star's atmosphere could be considered constant it will emitt as a black body with that temperature.

During radiative transfer, atmospheric layers will absorb radiation through bound-bound process in a molecular or atomic system, will reemit the radiation and scattering processes will redistribuite the energy. Scattered light will disappear along the direction of observation creating a drop of intensity and therefore lines formation in the spectrum.

Considering just absorption-emission processes the radiative transfer equation can be written

$$I_\nu(h) = I_\nu(h_0)e^{-\tau_\nu(h_0,h)} + \int_{h_0}^{h} B_\nu(T(h'))\alpha_\nu(h')e^{-\tau_\nu(h',h)}dh', \qquad (1.2.16)$$

This equation is the sum of two terms. The first is the Lambert-Beers' equation that describes intensity deecrese when radiation crosses a layer of

thickness $h$ and absorption coefficent $\tau$ of the material sample. It represents the part of the spectrum known as "continuum".

The second term $B_\nu(T) = \varepsilon_\nu/\alpha_\nu$ is the ratio between emission and absorption coefficient at the temperature $T$.

### 1.2.3 Stellar Opacity

Depending on temperature and density variation with height different stellar layers will show different behavior and properties. How much radiation reaches a spectrometer on earth from the core of a star depends upon what is in the outer layers it has to pass through. A measurement of how difficult it is for the radiation to travel through these layers is called opacity.

#### Opacity in the continuum

Opacity is the resistance that atmospheric layers make to the passage of electromagnetic radiation coming from the stellar interior strata. This property striclty depends on physical conditions and chemical abundances. For example, the temperature is lower in outer stellar layers, this increases the abundancies of atomic and molecular species and as a result the opacity is greater. We begin by describing how the energy flux varies with the as yet undefined measure of opacity.

We need to have some way of quantifying the property of opacity. Considering the radiative transport equation (1.2.16) between two adjacent layers at distance $\Delta h$ apart with temperature difference $\Delta T$ we can define the flux mean opacity as:

$$F_{\nu,h} = F_{\nu,0} e^{-\kappa_\nu \Delta h}, \tag{1.2.17}$$

where $\kappa_\nu$ is called the absorption coefficient and is such that the layers will have a distance of optical depth $= 1$ when $\kappa_\nu = 1/\Delta h$.

The Stefan-Boltzmann law can be derived from Planck's equation (1.2.10) for black body radiation and says that energy flux density is proportional to

temperature to the power four:

$$F_{h_0 \to h} = \sigma T^4. \tag{1.2.18}$$

$$F_{h \to h_0} \cong \sigma T^4 + \frac{\Delta F_{h_0 \to h}}{\Delta T} \cong \sigma T^4 + 4\sigma T^3 \Delta T, \tag{1.2.19}$$

We define the flux mean opacity as

$$\begin{aligned} F &= F_{h \to h_0} - F_{h_0 \to h}, & (1.2.20) \\ &= -4\sigma T^3 \Delta T, & (1.2.21) \end{aligned}$$

Comparing equation (1.2.16) with (1.2.21) and differentiating respect to $\nu$ we find that

$$F_\nu = -\frac{16}{3} \frac{\sigma}{\kappa_\nu} T^3 \frac{\mathrm{d}T}{\mathrm{d}h}, \tag{1.2.22}$$

where $T$ is the temperature, $\sigma = ac$ with $a = 8\pi 5k^4/15c^3h^3$, $\kappa_\nu$ is the absorbtion coefficient,$k$ is the Boltzmann constant, $c$ is the speed of light and $h$ the depth.

The variation of temperature of brilliance with wavelength allows us to tell which depth the radiation is coming from (see Figure 1.2). Infact, the temperature decreases going towards outer star layers *i.e.* $\mathrm{d}T/\,\mathrm{d}h < 0$. Analysing the intensity profile of the radiation at a certain wavelength, it is possible calculate the depth $h$ using the equation (1.2.22).

Atmospheric models can therefore be constructed using the temperature $T$ and density $\rho$ at different heights $h$ as input and the abundances varied until computed spectrum and observed coincide.

### Line-opacity

We have described the energy flux parameterised in terms of the opacity of the material $\kappa$. The absorption and emission of light by the material is

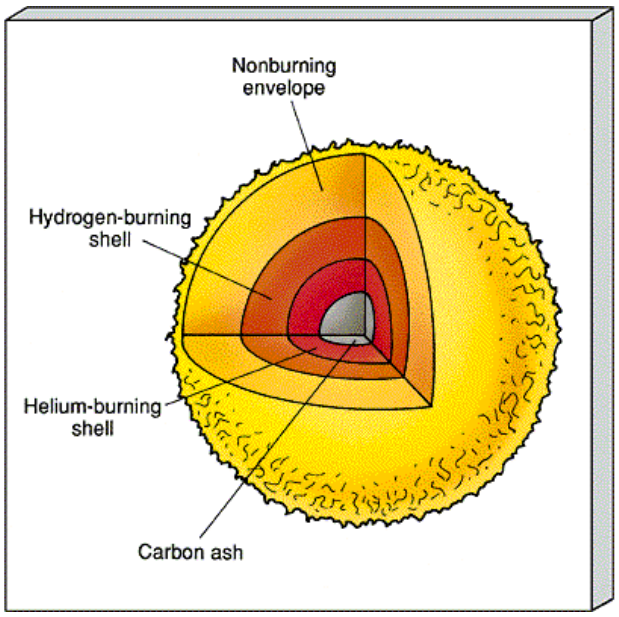


Figure 1.2: Layers of an Asymptotic Giant Branch AGB (taken from *www.shef.ac.uk*)

determined by the quantum mechanics of the atoms it is made out of. A material system subjected to irradiation will absorb the photon changing its energy status. A bound-bound interaction happen when the photon will be reemitted without causing any ionizzation or electron emission.

An atom in the outer layers of a star when hit by a photon of a specific frequency will change its energy level inside an atom by a specific amount. This absorbtion is known as line-opacity.

Assuming a local thermodynamic equilibrium the energy transport mechanism can be described by the MaxwellBoltzmann distribution:

$$\frac{N_m}{N_n} = \frac{g_m}{g_n} \exp\left(-\frac{\chi_{m,n}}{kT}\right), \tag{1.2.23}$$

where $g_i$ is the occupation number of the $i = n$ and $m$ levels, $\chi_{m,n}$ is the difference in energy levels, $T$ is the temperature, $k$ Boltzmann constant and $N_i$ is the occupation number of the energy level $i = n$ or $m$.

The Einstein coefficients are the emission, $A$, and absorption , $B$, probabil-

ities for spontaneous emissions between energy levels and are related to the occupation number as follows:

$$\frac{B_{nm}}{B_{mn}} = \frac{g_m}{g_n}, \tag{1.2.24}$$

$$\frac{A_{nm}}{B_{mn}} = \frac{g_m}{g_n} F_\nu, \tag{1.2.25}$$

Therefore opacity is not a directly observable quantity but is instead determined by the energy levels and occupation numbers (or Einstein coefficients) of the constituent parts of an atmospheric layer.

### Line strength

When the radiation electro-magnetic field interacts with dipole moment of the molecule and produces a transition. The line strengh associated with this transition is

$$S(m \leftarrow n) = \sum_{\phi_m, \phi_n} \sum_{A=X,Y,Z} |< \phi_m \mid \widehat{\mu_A} \mid \phi_n >|^2, \tag{1.2.26}$$

where $\phi_m$ and $\phi_n$ are eigenfunctions corresponding to energy levels $E_m$ and $E_n$. $\mu_A$ is the dipole moment operator with respect to the $A = X, Y, Z$ molecular coordinate system.

The notation

$$\int \phi_m^* O_p \phi_n \, \mathrm{d}^3 r = |< \phi_m \mid \widehat{O_p} \mid \phi_n >| \tag{1.2.27}$$

denotes the transition moment integral where $O_p$ is the transition moment operator. The transition moment operator represents a function that operates on a quantum state represented by wavefunction $\Psi_n$ to reproduce another state $\Psi_m$. Note that the squares of the absolute values $\mid \Psi \mid^2$ gives the probability distribution that the system will be in any of the possible states. In this case this operator is the molecular dipole moment and performs the transition between two vibro-rotational state of a molecule.

Note also that

$$\sigma \propto |< \Psi_m \mid \widehat{O_p} \mid \Psi_n >|^2 \propto A_{mn}, \tag{1.2.28}$$

where $\sigma$ is the cross section (in this case it represents absorption probability of photons by molecules) and $A$ is the Einstain coefficient. So the intrinsic line strength will be proportional to both $\sigma$ and $A$.

The absorption coefficient is calculated under thermal equilibrium approximation using the equation

$$I(m \leftarrow n) = \frac{8\pi^3 N_A}{(4\pi\varepsilon_0)3hcQ} S(m \leftarrow n), \tag{1.2.29}$$

where $h, c, k, N_A, \varepsilon_0$ are respectively Planck's constant, the speed of light, Boltzmann's constant, Avogadro's number and magnetic permeability in vacuum. $\nu_{nm}$ is the transition wavenumber ($\mathrm{cm}^{-1}$) corresponding to the energy levels $E_m$ and $E_n$ and $Q$ the partition function describing the statistical properties of a system of particles in thermodynamic equilibrium at temperature $T$ distribuited over $w$ energy levels $E_w$ with degeneracy factor $g_w$. Its expression is given by

$$Q = \sum_w g_w exp(-\frac{E_w}{kT}). \tag{1.2.30}$$

### Line Lists

A line list is a measure of opacity at a given wavelength and gives a molecule's "fingerprint". In a situation where no "fingerprint" is available for a molecule (it exists only in a star for example) then we can work back from a line list of a star and consider the quantum properties of the molecule.

A spectral line originates in the photosphere of a star and its absorption is usually measured relative to the flux mean opacity over the continuum. Line absorption contributes largely to the integral over the whole spectrum and for this reason can be considered a pseudo-continuous opacity source.

Using a line list it is therefore possible calculate molecular abundancies in a star. However, in order to interpret a star's line list an accurate representation of a line list for each molecule must be available. As we shall see, in the case of $C_3$ (which is not abundant on earth) such a line list must be calculated theoretically.

#### Weak Lines

For higher energies where the number of absorption systems in a particular spectral range is fewer, the line absorption coefficient will be relatively small and its drop in intensity will produce a weak line.

It turns out that even though they are weak, these lines play an important role and must be included in any reliable atmospheric model. Even though weak lines do not significantly contribute to the absorption coefficient integrated over the whole spectrum, they can change the stellar model atmosphere structure by several orders of magnitude due to the relatively big change of the (still weak) absorption in selected intervals of the spectrum (see Jorgesen *et al.* [2]).

The next section will describe evolutionary processes in stars. It is necessary to understand these processes in order to better describe stellar spectra features.

## 1.3 Stellar Evolution

In this section the life cycle of a star is described along with the associated changes in spectra observed.

### 1.3.1 The Beginning – A Dust Cloud

Material in the universe such as: simple molecules, grains and crystals is constantly subject to random fluctuations in pressure and temperature. This

material can be locally compressed by an increase of pressure and may become dense. When the preassure is released the material tends to disperse.

This continuous compression and rarefaction motion can sometimes develop into a growing instability where the increase of density is maintained and enlarged. In fact, attraction between molecules or grains is governed by two fundamental forces

- **Gravitational law** The force between two bodies $F_{GRAV}$ is given by

$$F_{GRAV} = G\frac{mM}{r^2}, \tag{1.3.1}$$

  where $m$ and $M$ are the masses of the two bodies respectively, $r$ is the distance between them and $G$ is the gravitational constant.

- **Pressure** The force due to the change in pressure $p$ with radius is given by

$$F_{PRESS} = -\frac{m}{\rho}\frac{\mathrm{d}p}{\mathrm{d}r} \tag{1.3.2}$$

  where $\rho$ is the density of the material.

These forces balance so that:

$$\frac{dp}{dr} = -G\frac{\rho M}{r^2} \tag{1.3.3}$$

### 1.3.2 A Protostar

During the emission processes (as energy is being radiated away) where temperature and internal energy and therefore pressure decrease, equation (1.3.3) says that the gravitational force must increase to try to contrast this reduction in pressure. This means that more material from the surroundings fall to the centre of this newly formed spherical gas cloud which is called a Protostar. The gravitational energy diminishes as a consequence of material contraction and the difference is converted in internal heat.

### 1.3.3 Pre-Main Sequence and T Tauri

When the contraction process slows down, the energy is transported from the centre to the surface largely through the convective motion outlined in Section 1.2.2.

During this stage, called pre-main sequence, a star's luminosity is high enough to let it be detected. Its irregular variability (due to a structural stabilization process still ongoing) together with other characteristic parameters allow it to be recognized and classified as T Tauri.

### 1.3.4 Main Sequence

Gravitational contraction raises core density and temperature up to critical values where nuclear reactions occur.

#### Nuclear Fusion

Hydrogen (H) fusion into helium (He) can occur through two different processes:

- **PP process** Conversion of hydrogen into helium through three different branches where the last two produce berillium.
- **CNO process** Conversion of hydrogen into helium through a combination of carbon (C), nitrogen (N) and oxygen (O).

The energy realized from the reaction that converts hydrogen into helium is enough to balance the amount dispersed in the interstellar medium through the surface and the gravitational contraction arrests.

The star then reaches a stable phase where there is a balance between internal pressure and gravitational attraction. As we see from (1.2.2) the star's effective temperature is determined by Luminosity $L$ and by its size $r$ which in turn is controlled by the gravitational internal pressure $p$.

### Effect of Initial Mass on Main Sequence

A star's evolutionary curve maps how surface temperature and luminosity vary with time. This curve will cross the H-R diagram (discussed in Section 1.2.1) at a certain position depending on the initial mass of the gas cloud.

- For stars with masses less than 0.05 $M_\odot$ (where $M_\odot$= solar mass = $1.9889210^{30}$ kg), core temperatures will never be high enough to activate nuclear reactions and gravitational contraction will increase drastically in density toward the centre. Electrons in the core will occupy, in pairs, the lowest energy state available and they will be frozen into a kind of crystalline pattern. When a total degenerate state is reached, no internal heat is produced, contraction stops and protostars go directly into the white dwarf stage without passing through the main sequence.
- Rare stars with masses greater then 50 $M_\odot$ will not go through the main sequence stage. They are identified as supermassive objects with evolution tracks that are still not clear.

The evolutionary curves of stars not included in the above mass ranges will cross the main sequence at a point depending on their mass with a certain chemical composition and radius kept almost constant during their time on main sequence.

Those points in the evolutionary curve at which the star contraction ends and hydrogen burning starts define the zeroage main sequence.

### Heat Transport Behaviour

Mass is also the decisive parameter in determining the heat transport behavior (see Section 1.2.2) during a star's time in main sequence. In stars with mass greater than 1.7 $M_\odot$, the heat transport is radiative in the envelopes and convective in the core. For a mass smaller then 0.4 $M_\odot$ the heat transport is totally convective. Stars is formed by superficial concentric layers over the core. These are:

- Photosphere
- Chromosphere
- Corona

Solar-type stars have convective envelopes and a lower surface temperature; they can present chromospheres and coronas accompanied by stellar wind.

### 1.3.5 The Red Giant Branch

After billions of years the hydrogen in the core of a star is exhausted and it no longer has a source of nuclear energy to balance the gravitational contraction. In stars with masses:

- $M < 1.4$ $M_\odot$ H-burning processes are faster due to the higher values of temperature and density in the inner stratus. This will lead to the formation of an inert helium core surronded by an external area where the reactions are still active. An isotermic status is instaured and central density enhances to contrast external pressure. The density grow is balanced by core degenetation. Luminosity will increase and convective motions are responsible for processess called dredge-up where material is stirred and reaction products will be transported in superficial layers.
- $1.4M_\odot < M < 2.5M_\odot$ hydogen burning rate is constant in all parts of the core thanks to the convection material stirring and this lead to the formation of an isotermic helium core. Central density is enough to let core degenerate and the star will evolve towards white dratf stage as low massess stars does despite chemical composition omogeneity is typical of star with greater value of mass.
- $M > 2.5M_\odot$ when the helium core will reach the Schomberg-Chanrasecar limit the core will contract rapiditely and the temperature increases up to activate (ignite) hydrogen burning in a shell around the helium core. The radius of the stars envelope increases drastically. Stars will reach a Luminosity of 2500 solar luminosity $L_\odot = 3.827 \times 1026W$ and temperature of 4000 K and will reach the Red Giant Branch (RGB) in

the H-R Diagram. The degenerate core will heat up until reaching a temperature of $10^8$K. This temperature is high enough to ignite helium burning with a growing efficiency of carbon production due to the decoupling between temperature and pressure. A stable helium burning core will be established thanks to thermal a runaway process known as the helium flash that removes the core degeneracy. A diagram of this is shown in Figure 1.2

### 1.3.6 The Asymptotic Giant Branch

The star's evolution curves leave the main sequence in the H-R diagram marking an horizontal line towards inferior effective temperature and almost constant luminosity called the Horizontal Branch. When helium is totally converted into carbon, the inert carbon-rich core will contract again and became degenerate. Those stars with a degenerate core mass beyond a certain limit called Chandrasekhar limit of $1.4M_{\odot}$ are able to balance gravitational contraction.

Stars luminosity and radius increase as consequence of helium and hydrogen burning in shells around the star core. They will then move up in the H-R diagram to the Asymptotic Giant Branch (AGB).

### 1.3.7 Pulsars

Hydrogen burning will increase the mass of the helium shell (He-shell) and helium burning causes a degenerate environment. Thermonuclear runaway processes will be responsible for what is called a 'Thermal Pulse' in which luminosity and radius will increase and the temperature will decrease to below the value necessary for hydrogen burning. Convective motion will extend to the inner regions causing a dredging up of carbon atoms towards the outer atmospheric layers where carbon will then become dominant over oxygen and the H-shell will continually supply the necessary quantity of helium for next Thermal Pulse.

This process will cause a star's mass to decrease and its H-shell to become unstable and start to pulsate.

### 1.3.8 Planetary Nebula and White Dwarfs

When the envelope mass decreases to under 0.001 $M_\odot$ the mass loss ends and superwinds will obscure totally the star. In the H-R diagram the star will move towards the Post-AGB phase where the AGB outflow will form a planetary nebula. Finally as the core cools down at constant radius is known as a white dwarf.

### 1.3.9 The End? – Neutron Star or Black Hole

Stars with an initial mass grater then 8 $M_\odot$ will carry on with carbon-burning up to silicon to iron burning. When the iron core mass has exceed the Chandrasekhar limit, it will collapse forming a neutron star or a black hole.

## 1.4 Cool Carbon Rich Stars and Stellar Opacity

Stars which are carbon rich and have an extended atmosphere (those in the Asymptotic Giant Branch (AGB) stage) have very low densities and their photospheres are cool enough (about 4500 K) to allow molecules to form.

An example of these characteristics can be found in those stars classified as the Mira variable type. These also present other peculiarities such as: brightness in the infra-red spectrum; pulsations; mass loss; emission lines for (hydrogen, silicon and iron); absorption lines (metals) and molecular absorption bands.

A very peculiar and interesting dynamics exists in the atmospheres of stars during AGB evolution phase. Energy from the inner layers is transferred to external layers by convection cells (as discussed in Section 1.2.2). This creates irregular pulsations with shock waves propagating towards the surface where matter is expelled as wind.

As a consequence spectra of AGBs atmosphere are very complex showing an enormous numbers of atomic and molecular lines. A radiative-hydrodynamic

model inclusive of coupling effects between convective motion, radiation and instability effects is necessary to explain asymmetry in the line profile, time variability (a blue absorption component appears as a progressive shift to the red as a consequence of a shock wave in the line forming region) and doubling effects. Theoretical calculations can support the observations, not just predicting the lines position but also giving fundamental coefficients (such as intensities) [3].

This report presents the preliminary work carried out to perform a computational study of the $C_3$ system in order to obtain an accurate and complete line list to test against experimental results and astronomical observations of AGBs.

# Chapter 2

# Molecular Properties of the $C_3$ Molecule

In recent years, there has been increasing interest in pure carbon molecules, sometimes referred to as polycarbons or $C_n$ (see for example Weltner and Van Zee [4]). New experimental methods have been developed to study the quite peculiar and complex spectroscopic properties of these $C_n$ species up to $n = 200$.

At the moment, there are just a few observations of $C_n$ species in space. $C_3$ and $C_5$ have been detected in comets, diffuse interstellar medium and in the circumstellar shell of some late type giant carbon stars (see Section 1.3).

The $C_3$ molecule plays an important role in the growth of carbon chains and the determination of its abundance in the interstellar and circumstellar media could improve our understanding of the chemistry prevailing in these objects [5].

The $^{12}C_3$ molecule is formed by three symmetrically equivalent bosons nuclei this means that the total spin of the particles forming nuclei of carbon is an integer.

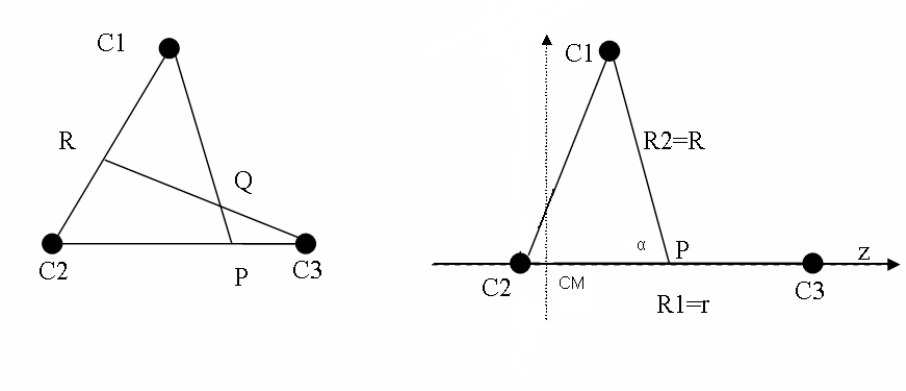


Figure 2.1: The generalized internal coordinate system of Sutcliffe and Tennyson [6] left, and Jacobi coordinates with $z$ embedding chosen to study $C_3$.

## 2.1 Coordinate Systems and Notation

Before looking at the properties of the molecule it is important to establish the various notations and coordinate systems used:

### Notation

### Coordinate Systems

It is convenient describe the molecule using a Cartesian coordinates reference system $(x, y, z)$ centerd in the centre of mass of the molecular system as shown on the right side of Figure 2.1.

Symmetric and antisymmetric stretch coordinates coordinate system is $(X_1, X_2, \theta)$ with $X_1 = q_1 + q_2 - 2re$ is the symmetric stretch coordinate, $X_2 = q_1 - q_2$ is the antisymmetric stretch coordinate where $q_1$, $q_2$ are the two bond-lengh, $\theta$ the angle between bond-lengh and $r_e$ is the bond-lengh at equilibrium configuration.

Jacobi or scattering coordinates $r$, $R$ and $\alpha$ are $r = q_2$, $R$ is the distance between $q_2$ centre of mass and the other carbon atom Figure 2.1.

| NORMAL MODE | SYMMETRY SPECIES [*] | DESCRIPTION | BAND TYPE | FREQUENCY (cm-1) | SELECTION RULES | DIPOLE MOMENT (Debye) |
|---|---|---|---|---|---|---|
| C=C=C V1 | $\Sigma g+$ | SYMSTRETCH | RAMAN, | 1224.4933[1] | Δv=±1, ΔJ=0,±2 Stocks-AStocks | / |
| C=C=C V2 | $\Pi_u$ | BEND (double degenere) | FIR, | 63.41653[2] | Δv=±1, ±2,..... ΔJ=0, ±1 PQR | 0.19[3] -0.44[6] ? |
| C=C=C V3 | $\Sigma_u+$ | ASYMSTRETCH | IR, | 2040.019[2] | Δv=±1, ±2,..... ΔJ= ±1 PR | 0.44[3] -0.35[6] ? |

[*] Σ modes involving parallel vibrations (z)
Π modes involving perpendicular motion double degenere (x,y)
g, u retain/not retain the centre of inversion symmetry
+, - reflection symmetry

[1] G.Zhang et al. 2005, J. Of Chemical Physics 122, 244308.
[2] K.Kawaguchi et al. 1989, J. Of Chemical Physics 91,1953.
[3] W.P. Kraemer et al. 1984, J. Mol. Spectr. 107, 191.
[6] Per Jensen 1993, J. Mol. Spectr. 97 (5).

Figure 2.2: C3 Fundamental modes

## 2.2 Rotation-Vibration Spectra

Using Infrared Spectroscopy (IR) (see Section 1.1) it is possible to study the vibrational and rotational frequencies of triatomic molecules which correspond to discrete energy levels. We discuss each of these in turn.

### 2.2.1 Vibrational Frequencies

A molecule with $n$ atoms can vibrate in $3n-6$ normal modes. Linear triatomic molecules have $3n-5$ modes (if $n=3$ it has 4 in principle vibrational modes) Figure 2.2 . We label these:

- Symmetric-stretching (parallel to the linear axis)
- Anti-symmetric stretching (parallel to the linear axis)
- Bending (perpendicular to the linear axis and double degenerate).

In terms of spectra (working in a cartesian coordinate system $(x,y,z)$ relative to the molecule with z axis embedded parallel internuclear distance $q_2$ ) these vibrational modes are called:

- Parallel bands: The anti-symmetric and symmetric stretching motion parallel to the $z$ molecular axis.
- Perpendicular bands: The double degenerate perpendicular bending motion along $x, y$ axes.

Whitin the harmonic oscillator approximation, vibrational energy levels of a molecule are given by:

$$E\left(\nu_i\right) = \sum_i h\nu_i \left(\nu_i + \frac{d_i}{2}\right), \tag{2.2.1}$$

where $d_i$ is the degeneracy of the $i^{\text{th}}$ mode with frequency $\nu_i$ and $h$ is Planck's constant.

A simple way of describing vibrational motions is to treat them as harmonmic oscillator systems with actual potential energy and dipole moment functions depending on the distance between atoms. Real molecules, however, are more complex systems and the vibrations posses an anharmonic features. The analytical forms used to describe their motion have to be chosen taking into account molecular chemical properties and geometry.

Harmonic oscillators have selection rules $\Delta\nu = \pm 1$ with fundamental vibrational band $\nu = 1 \leftrightarrow 0$ and hot bands (transitions between excitated levels) $\nu_{i+1} \leftrightarrow \nu_i$ with $\nu_i \neq 0$.

Molecules which posses anharmonic oscillations have overtone transitions with selection rules $\Delta\nu = \pm 2, \pm 3, ...$ are allowed but generally much weaker then fundamental transitions.

The harmonic oscillator model presents fundamental modes and also a conbination of them $\nu_i + \nu_j$ with $i \neq j$ and conbination transitions rely on anharmonic effects.

A molecule shows rotational transitions if it possess a dipole moment, vibrational ones require a change in dipole. The magnitude describes the electrical properties of a molecular system:

$$\vec{\mu} = q\vec{r}_i, \tag{2.2.2}$$

where $q$ is the charge and $r_i$ is the charge separation.

Polyatomic molecules dipole moments can be expressed using analytical function. An example of functional form for one mode in a diatomic molecule is:

$$\mu\left(r_i\right) = \mu_e + \frac{d\mu}{dr_i}\mid_{r_e}\left(r_i - r_e\right) + \frac{1}{2}\frac{d^2\mu}{dr^2}\mid_{r_e}\left(r_i - r_e\right)^2 + \cdots, \tag{2.2.3}$$

where $\mu_e$ is the permanent dipole moment and the other terms express the higher order dependency with internuclear separation. Molecules can have

- $\mu_e = 0$ **and** $\dfrac{d\mu}{dr_i} = 0$ Dipole moment is zero and molecules do not show IR transitions (for example homonuclear diatomic molecules).
- $\mu_e = 0$ **and** $\dfrac{d\mu}{dr_i} \neq 0$ Molecules show roto-vibrational transitions but no pure rotational spectra.
- $\mu_e \neq 0$ **and** $\dfrac{d\mu}{dr_i} \neq 0$ Molecules have ro-vibrational and pure rotational transitions.

### 2.2.2 Rotational Frequencies

Molecular rotation can be described by considering a reference system $(x, y, z)$ with the centre of mass at the origin and its moment of inertia about those axes

$$I_p = \sum_i m_i r_{ip}^2, \tag{2.2.4}$$

where $p = x, y$ or $z$, $m_i$ is the atom's mass and $r_{ip}$ the distance from the axes $p$.

Molecules can be then be classified in terms of their inertia as

- **Linear molecules** $I_x = I_y, I_z = 0$.

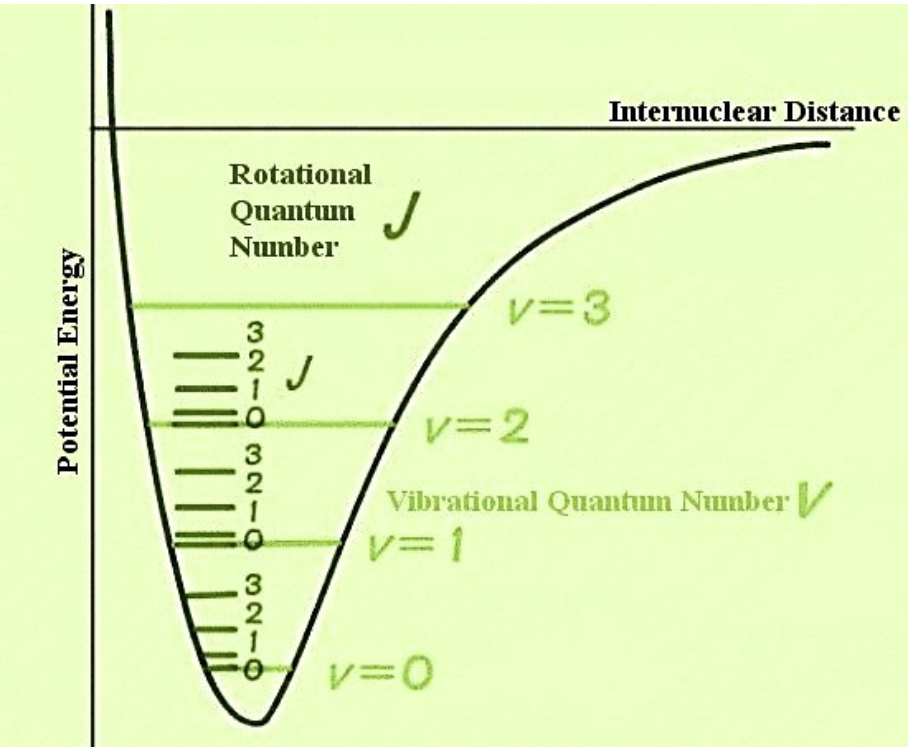


Figure 2.3: Schematic representation an 1-dimensional Potential Energy function and vibrational and rotational energy levels.

- **Spherical Top** $I_x = I_y = I_z = 0$.
- **Symmetric Top** $I_x = I_y \neq I_z$.
- **Asymmetric Top** $I_x \neq I_y \neq I_z$.

Within the rigid rotor approxiamtion the rotational energy levels of a closed shell linear molecule is given by

$$E_{rot} = BJ(J+1), \tag{2.2.5}$$

where $B$ is the rotational constant measured in MHz and $J$ is the rotational quantum number $0, 1, 2, 3....$ Figure 2.3.

Selection rules are $\Delta J = 0, \pm 1$ or labelled as Q P R branches when associated with vibrational transitions. Vibrational perpendicular bands present P

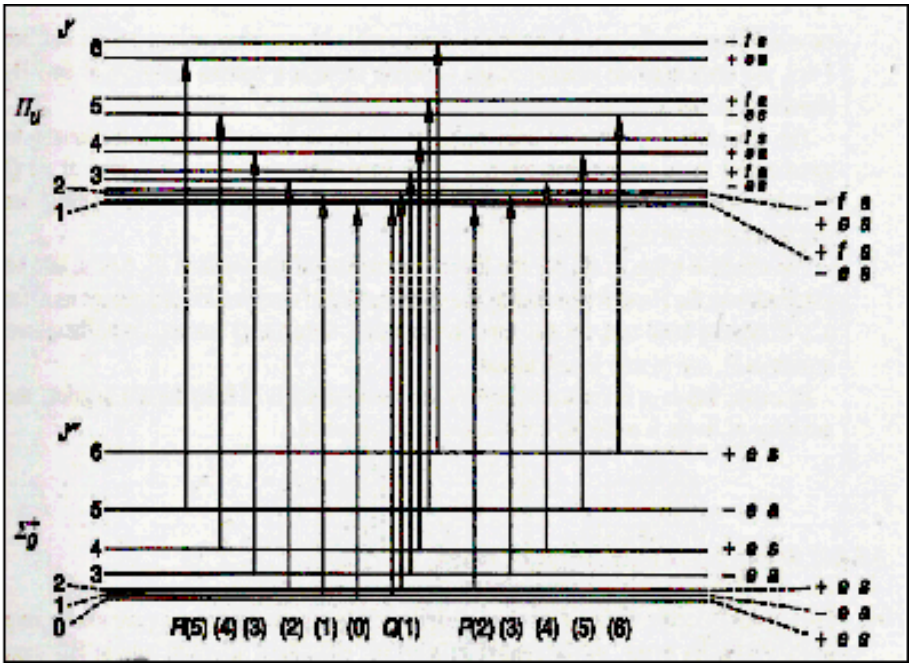


Figure 2.4: Vibrational and rotational energy levels including l-doubling effect for a transition between .

and R branches and parallel band PQR. More, degenerate vibrational modes (bending modes of a linear molecula for example) possess a vibrational angular momentum $\vec{l}$ and the spectrum shows an $l$-doubling effect due to the coupling between vibrational and rotational quantum number:

$$\vec{J}_{TOT} = \vec{J}_{Rot} + \vec{l}, \tag{2.2.6}$$

with $\mid l \mid = \nu, \nu - 2, .....1$ or 0 for a degenerate bending frequency $\nu$.

## 2.3 Symmetry Properties

$^{12}C_3$ possess a center of symmetry and is formed by three symmetrically equivalent Bosonic's nuclei. A consequence of this is "missing' lines in the

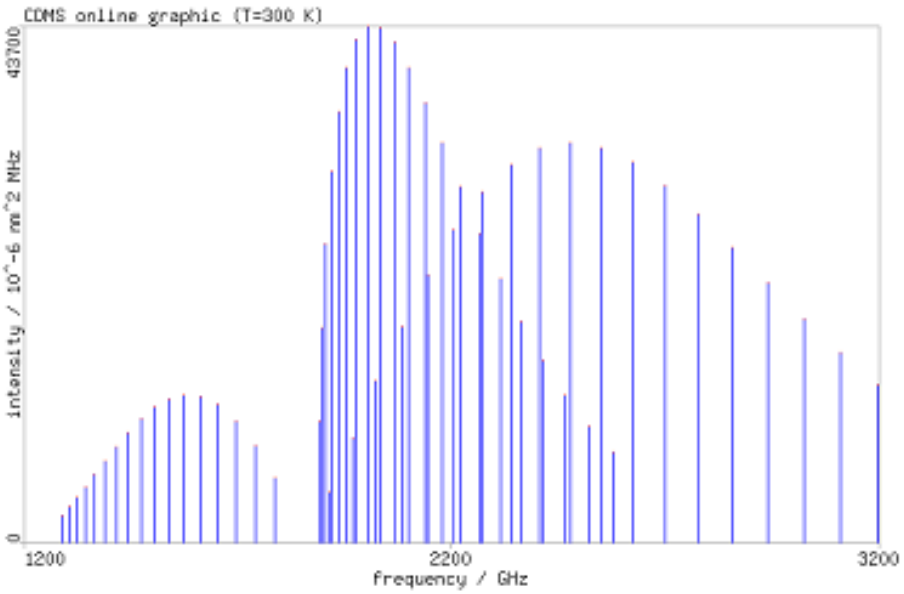


Figure 2.5: Fundamental bending mode of $C_3$ at 63.4166 $cm^{-1}$. Spectrum by R.Gendriesh et al. 2003, Z. Naturforsch. 58a,129.

observed spectra. To understand this particular behavior, we should briefly look at the symmetry properties and statistics of the $C_3$ system.

Using the Born-Oppenheimer approximation and separating vibrational and rotational motion we can see that the complete wave-function $\psi_{TOT}$ is a product of the electronic $\psi_e$, vibrational $\psi_v$, rotational $\psi_r$ and nuclear spin $\psi_n$:

$$\psi_{TOT} = \psi_e \psi_v \psi_r \psi_n. \tag{2.3.1}$$

The total wave function must be symmetric because carbon atoms follow Bose Einstein statistics. The ground electronic wave-function is symmetric as is the nuclear one; it follows that the product between rotational and vibrational part must be symmetric too.

As both the vibrational and rotational wave functions are symmetric, the

spectra "misses" the lines that arise from states associated with an antisymmetric rotational-vibrational wave-function.

An example is shown in the Figure 2.4. This shows the ro-vibrational transition between the ground vibronic state and the fundamental bending band with the vibrational angular momentum $l = 1$ and where just the lines with $J$ =even are observable.

The parameter $l$ describes the vibration angular moment which increases when the molecule is more bent.

The low fundamental bending frequency (*i.e.*extreme floppiness) of $C_3$, results in a very large $l$-doubling. In the linear configuration, degeneracy in $l$ is observed. As the molecule becomes more and more like an asymmetric top this degeneracy is increasingly broken.

In conclusion, although $C_3$ is a linear molecule, it is possible treat it as a special case of an asymmetric top and the $l$-doubling can be handled like the $k$-doubling (this is the doubling caused by the projection k of molecular angular moment J along the rotation axe) in an asymmetric top. This means that calculations can be carried out using computer programs written for the calculation of the vibration-rotation spectra of non-linear triatomic molecules provided this program treats the transition from non-liner to linear geometry correctly.

## 2.4 Linear or Quasilinear Equilibrium Geometry?

An interesting problem for $C_3$ is determining its equilibrium geometry structure.

Moleculas can be linear, nonlinear or quasilinear. The first two are self-explanatory. A molecule with quasilinear structure has a bent equilibrium structure but vibrates through the linear configuration even in its vibrational ground state [7].

For $C_3$, early CI-SDQ calculations (a method using Configuration of Iteration

with single, double and quadruple excitation) performed by Kramer *et al.* [8] predicted a slightly bent equilibrium geometry with an equilibrium angle of 161.6 ° and an effective bending potential that shows a linear configuration in state ($v_1, v_3 = 0$) and bent in ($v_1 = 0$, $v_3$) (as result of strong bend-stretching coupling).

Molecules with "floppy" large amplitude vibration may present a large $l$-type doubling indicating a strong rotation-vibration coupling. As a consequence, present fascinating features such as:

- Barriers to linearity.
- Mixing between levels of the same $J$-rotational quantum number and different values of $l$.
- Inversion and splitting (resolving) of degenerate levels appearing when calculting ro-vibrational energy levels.
- Anarmonicity.
- Coupling effects.
- Mixing and inversion of energy levels.

Bunker [7] introduced a semi-empirical numerical method "Semi-rigid Bender Analysis" to determine the structural configuration of a molecule by analysing the shape of electronic PES. Also it has been found that energy level splitting behaviour can be a good structure index.

Liskow *et al.* [9] [4] have demostrated the importance of $d$ functions (that are functions representing the electrons's occupation of d orbitals) in describing correctly the bending behaviour. A surplus of $d$ function can lead to an incorrect bent equilibrium geometry of $C_3$ and the same thing will happen when adding the Davidson corrections (that allows one to estimate the full CI contribution from a set expanding a limited set of extimators)(see Kramer *et al.* [8]).

Experimental studies due to Nortrup and Rolphing [10, 11] analyse respectively the bent-symmetric-stretch $(v_1, v_2, 0)$ and the bend-antisymmetric-stretch $(0, v_2, v_3)$ combination levels.

A Semi-rigid Bender Analysis also performed by Nortrup and Rolphing [12] demostrated a linear equilibrium geometry. They analysed the $J = 2$ splitting between $l = 0e$ and $l = 2e$ (sigma-delta splitting). They show that the experimental splitting decreases as $v_2$ increases. Also in $v_1$ states the $\sigma$ ($l = 0$) and $\delta$ ($l = 2$) state are inverted relative to the stretching to the ground state.

Nortrup and Rolphing therefore propose that a potential that exitbits a barrier to linearity cannot reproduce the small splitting (*i.e.*the low bending vibrational frequency ). They therefore conclude that $C_3$ is linear.

In fact, as Jensen reported, the $l$-splittings in the rotational structure of a given vibrational level are extremely sensitive to details of the potential surface [10]. AHM PES (PES calculated by [13]) was built using the MRCI method MultiReference Configuration Iteration method including Davidson correction. As result the $l$-splitting is too small in comparison with the experimental result.

As shown the AHM potential energy surface is apparently flat Figure 2.6.

In this thesis we propose that the $C_3$ molecule could have a linear geometry at the equilibrium but ground state vibrational motion vibrating through bent configuration. In the next chapter this proposition will be tested.

## 2.5 Experimental Research Into the Properties of $C_3$

Experimental research by Northrup and Sears [14, 10]; Northrup, Sears and Rohlfing [12]; Rohlfing and Goldsmith *et al.* [15, 11] show no barrier to linearity in the quite flat bending potential for either the zero point ($\nu_1 = \nu_3 = 0$) or the equilibrium stretching mode states of the $C_3$ molecule.

By contrast, they see that the molecule develops a barrier (of about 21 $cm^{-1}$ and a bond angle of 162.5 °) in the linear configuration as the anti-symmetric stretch is excited. Moreover, they observed a strong bend-stretch interaction in the ground state. This is very unusual for linear molecule where the rotational constant of the antisymmetric stretching should decrease as the

the vibrational excitation increases.

An opposite trend is more usually observed where the molecule becomes more rigidly linear upon symmetric-stretch and more floppy when anti-symmetrically stretched.

The experimental research of Northrup *et al.*suggests that, the dramatic rise in the rotational constant) as a function of the anti-symmetric stretching is correlated with the increasingly larger barrier to linearity in the effective bending potential. They suggest that: 'the shape of the potential is fairly insensitive to small changes in the bond length or with its variation with the bending angle and the dependence of the bond length on the bending angle is relevant'.

The type of absorption bands observed depend upon the direction in the rotating molecule of the oscillating electric dipole moment induced by the electromagnetic radiation (as discussed by Duxbury *et al.* [16]). In the symmetric stretching motion, there is no variation in the transition dipole moment; that means that it can be observed using Raman spectroscopy but not in IR. Raman spectroscopy techniques gives information about ro-vibrational features using scattering light from the molecular system. This allows to obtain information not displayed by IR spectroscopy.

The anti-symmetric stretching and bending fundamentals one are Far Infrared and Infrared active and they show PR (selection rules $\Delta J = +1$(P branch) and $\Delta J = -1$ (R branch)) and PQR (selection rules $\Delta J = 0$(Q branch)) types of absorption bands respectively the Q branch in the bending motion can be observed because a vibrational change can happen without a simultaneous rotational transitions.

Early theoretical studies by Kramer *et al.* [8] show a very high transition dipole moment for the $\nu_3$ band in comparison with the one for $\nu_2$ band. Recent laboratory experiments by Schmuttenmaer *et al.* [17] and theoretical studies performed by Jensen *et al.* [18] disagree with Kramer's theory and in fact show a similar fractional absorption for the two IR-active bands.

## 2.6 Summary

In summary the $C_3$ molecule has the following properties:

**Linearity of Structure** It has a linear or quasi-linear structure in its ground electronic state.

**Symmetry of Structure** It has a center-symmetric structure *i.e.*it posses a centre of inversion.

**Dipole Moment** does not have a permanent dipole moment so strong pure rotational transitions cannot be observed.

$\pi_g$ **Electrons** $\pi_g$ electrons are electrons in overlapping p-orbitals.

The bending frequency of a molecule is therefore related to the $\pi_g$ electrons as they act like a "backbone" [19]. The $C_3$ molecule does not posess any of these type of electrons and this leads to

**Low Bending Frequency** An unusually low bending frequency of 63.4165 $cm^{-1}$ (see Walsh [20]).

**Potential Energy** It has a relatively flat potential energy this means that at low frequency is already possible observe great vibrational displacements.

**Floppiness** Due to the low bending frequency the $C_3$ molecule presents a high degree of floppiness. Indeed, in the first exited state, where $\pi_g$ orbital is occupied, the fundamental bending frequencies go up at about 350 $cm^{-1}$ [19].

### 2.6.1 Use of Molecular Properties For Astronomical Observations

$C_3$ was observed for the first time by Higgins *et al.* [21] in emission from comets in 1882 and later by Hinkle [22] in absorption through its fundamental antisymmetric stretch band ($\nu_3$) in the atmosphere of the cool carbon star IRC +10216. This object is a carbon rich Mira variable with an unusually thick and dense dust molecular envelope. For this reason it gives a natural laboratory to understand the interstellar and stellar chemistry (see

Cernicharo and Goicoechea [23]).

In 2000, observations made by Cernicharo *et al.* [23] showed the detection of the low bending frequency, again in IRC +10216 and in a massive dense molecular cloud: Sagittarius B2 which is the richest concentration of molecule in the Milky Way. The detection of this unusual and quite low fundamental bending band opened new possibilities to detect other molecular species without a permanent dipole moment [5], *i.e.*lacking of pure rotational transitions.

Most recently Harris *et al.*detected the fundamental antisymmetric-stretch band $\nu_3$ in the outer atmosphere of cool AGB (Asymptotic giant branch) carbon star WZ Cas [24].

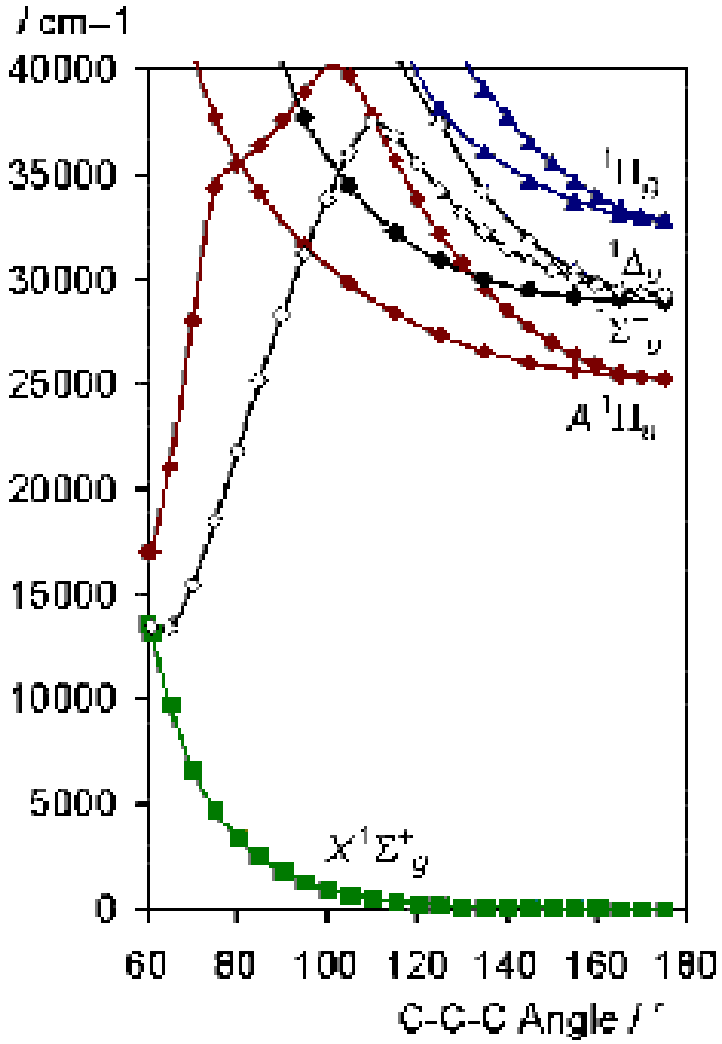


Figure 2.6: Potential energy surfaces for the ground and first excitated state as calculated by Ahmed *et al.* [13]

# Chapter 3

# Variational Approach to the Study of Triatomic Molecules

An already tested and successful approach to study the infrared spectra of molecules is the separation of the electronic problem from the nuclear one using Born-Oppenheimer's approximation. This approximation is based on the fact that electrons are thousand times less lighter than nuclei which allows setting nuclear kinetic energy to zero in electronic structure calculations.

As described by Jensen and Bunker [25] there are two ways of solving the bound state nuclear motion problem which arises as the second step in the BO approximation: the perturbation theory approach and the variation theory approach. The perturbational approach is based on studying a complex system approximating it to a simple one and find an approximate solution to the Schrodinger equations. Despite being useful for studying several systems, it is not well suited describing a molecule with large amplitude motion such as $C_3$. A variational approach is more suitable for studying $C_3$ characteristics and a description of this method will be given in the next sections.

### 3.0.2 The Wave Function Problem

Schrödinger's equation is used in quantum mechanics to determine allowed quantum states for microscopic and macroscopic systems. The time-independent

equation states that:

$$H\Psi = E\Psi, \tag{3.0.1}$$

where $H$ is the Hamiltonian Operator, $\Psi$ is the wavefunction of the particle, and $E$ is the energy of the particle.

The Hamiltonian operator $H$ of any system is given by the sum of its kinetic and potential energy. For $C_3$, working in Jacobi coordinates, the operator is written [26]

$$H(r_1, r_2) = K_v^1 + K_{vr}^1 + \delta_{k',k}\langle j'k|V(r_1, r_2, \theta)|jk\rangle_\theta, \tag{3.0.2}$$

where $V(r_1, r_2, \theta)$ is the potential energy function and $K_v$ and $K_{vr}$ are respectively the vibrational and the ro-vibrational kinetic energy operators. $\delta$ is the delta function (it takes the value zero for all $k \neq k'$).

Vibrational motions and their characteristic frequencies are determined using analytical functions known as Potential Energy Surfaces (PES) describing electronic energy interactions between atoms making up a bonded chemical system.

- **Radial basis** Symmetric and antisymmetric motions can be approximated using Morse-like functions [1]:

$$\mid n >= H_n(r) = \beta^{\frac{1}{2}} N_{n\alpha} exp(-\frac{y}{2}) y^{\frac{(\alpha+1)}{2}} L_n^\alpha(y), \tag{3.0.3}$$

with

$$y = Aexp[-\beta(r - r_e)], \tag{3.0.4}$$

where

$$A = \frac{4D_e}{\omega_e}, \beta = \omega_e(\frac{nu}{4D_e})^{\frac{1}{2}}, \alpha = integer(A), \tag{3.0.5}$$

where $r_e$ is the equilibrium distance, $\nu$ is the reduced mass, $\omega e$ is the fundamental frequency, $D_e$ is the dissociation energy and $N_{n\alpha}L_n^\alpha(y)$ normalized Leguerre Polynomials.

- **Angular basis** These are Legendre polynomials:

$$P_n(x) = \frac{1}{2^n n!}\frac{d^n}{dx^n}[(x^2-1)^n], \tag{3.0.6}$$

The potential energy surface (PES) $V(r_1, r_2, \theta)$ necessary to perform nuclear motion calculations can be constructed by estimating the electronic energy for each nuclear geometric configuration (using a program such as MOLPRO [27] for example). The quality of the PES sets the accuracy of the subsequent ro-vibrational calculations. For this reason, much experimental and theoretical effort has been focused on determining the right shape of the potential-energy function [18]. It is observed that the most accurate PESs are computed using ab-initio starting points, with the resulting surface being empirically adjusted to improve the agreement between the computed energies and experimental data [28].

Having constructed the PES the bound states of the system can be determined using as basis set of square integrable eigenfunctions (within Hilbert space) expressed as one-dimentional array form and the Hamiltonian $H$ in a matrix form. The equation can be solved by diagonalising the $H$-matrix and obtaining eigenvalues representing energy levels of the system. Increasing the set of functions forming the $H$-matrix, the eigenvalues will converge more and more to their exact value.

Highly floppy molecules motion is better decribed using a Discrete Variable Representation (DVR) matrix [26] obtained by performing an orthogonal transformation in which the basis function set is represented in a coordinate space rather than in a functional space. Sucessive diagonalzations and truncations lead to a reduction in the dimension of the analytical problem and computational time expences [26].

### 3.0.3 Computational Solution

A program has been written by Tennyson *et al.* [1] for performing nuclear motion calculations using variational techniques (this is refered to as the DVR3D program suite). It requires as input a prebuilt PES and preliminary

tests are necessary in order to determine if they are appropriate to carry out the calculations or if they need some adjustments.

DVR3D uses variational techniques, where the wave-functions $\Psi$ are defined by a complete set of weighted, orthogonal grid points expressed in Jacobi or Radau coordinates. The program uses Legendre polynomials as angular basis functions and either Morse oscillator-like functions or spherical oscillator as radial basis functions.

In the case of $C_3$, the linear equilibrium geometry encourages the use of Jacobi coordinates $R$, $r$ and $\alpha$ (see Figure 2.1) and Morse oscillator-like functions. These functions are defined in terms of parameters that must be optimized in order to achieve a balance between computer power, time expense and the convergence of all the energy levels (the aim for this work is 0.01 $cm^{-1}$ spectroscopic accuracy).

Due to the nuclear spin statistic of $C_3$, some rotation-vibration symmetry blocks are "missed", this means for $J$ even just ee (even-vibrational/even-rotational wave-function) and oo symmetry will be considered, and for $J$ odd just the eo and oe blocks.

DVR3D allows not just bound rotation-vibration energy level calculations but also wave-functions, expectation values and if a DMS is supplied, Einstein coefficients and temperature-dependent spectra. The calculations to obtain an accurate infrared line-list can be very expensive in terms of computer power and time, and test procedures are necessary to evaluate the quality and goodness of the PESs and DMSs inputted into the DVR3D program.

## 3.1 Potential Energy Surface

Recently, three-dimensional Potential Energy Surfaces for the carbon trimer have been constructed by fitting some ab-initio points calculated using the MOLPRO suite [27] program (see Mladenovic *et al.*. [29] (MLAD), Jensen *et al.* [18]) and Ahmed *et al.* [13] (AHM1)Figure 2.6).

Jensen's Potential energy surface is too bent to reproduce the l-doubling sigma-delta splitting and it will not be used to perform test and calculation

with DVR3D. The other two potential surfaces MLAD and AHM will be analysed and tested. Both surfaces $V$ have the following functional form:

$$V = \sum_{i,j,k} C_{i,j,k} X_1^i X_2^j \theta^k \tag{3.1.1}$$

where $X_1 = q_1 + q_2 - 2$ and $X_2 = q_1 - q_2$ are the symmetric and antisymmetric stretch coordinates respectively, $\theta$ is the bond-angle and $C_{i,j,k}$ are parameters obteined by MLAD and AHM by fitting the ab-initio points for calculate $C_3$ PES.

A large basis set have allowed the MLAD PES to reproduce energy levels up to 300 $cm^{-1}$, above the zero-point energy, with good agreement (a standard deviation of 7.3 $cm^{-1}$) with experiments.

The AHM1 pure ab-initio PES is not as accurate as MLAD's (it has an average error of 61.6$cm^{-1}$). Adjustments by a fitting of a few potential coefficients to the available experimental data enables the AHM1 Potential to give vibrational levels up to 8000$cm^{-1}$ with a standard deviation of 2.8 $cm^{-1}$ from the experimental data. A comparison between the two PESs is given in Figure 3.1 and Figure 3.2.

### 3.1.1 Energy Level Calculations Using the Mladenovic *et al.*. and Ahmed *et al.*. PES

The ro-vibrational energy level calculation with $J = 0$ obtained using MLAD and AHM1 PESs as input to the DVR3D program suite are shown in Table 3.1.

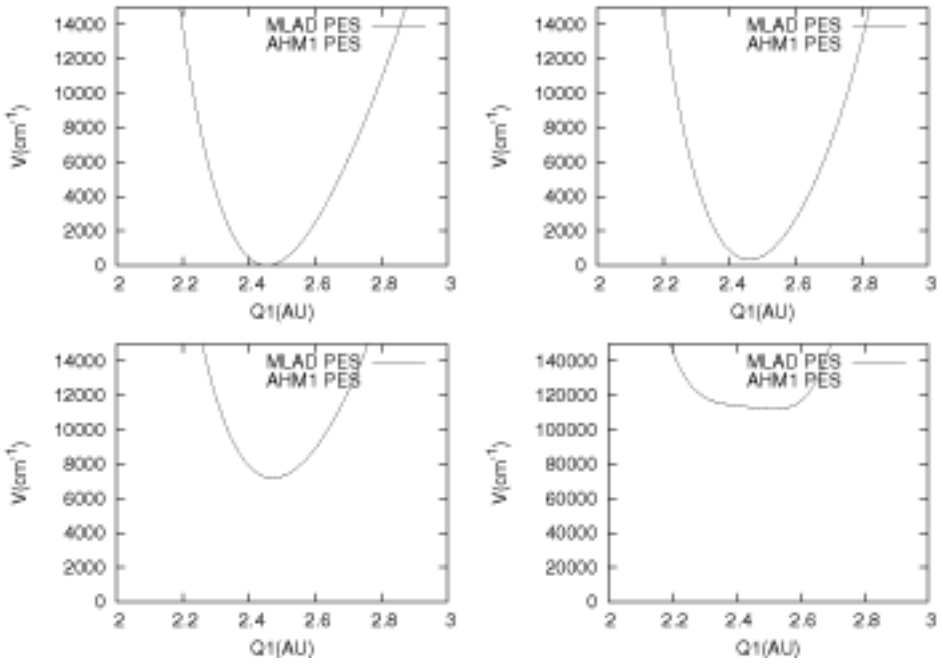


Figure 3.1: MLAD and AHM1 PESs as a function of the bondlength $q_1$. $q_2$ is fixed at the equilibrium values and $\theta$ from the left top assumes the value 10 °, 60 °, 90 °, 120 ° respectively

Table 3.1: Differences, in $cm^{-1}$, between the experimental [14, 15, 10, 11, 12, 30, 17, 31] and calculated vibrational energy levels. Calculations performed by Mladenovic [29] and Ahmed *et al.* [13] are compared with our DVR3D calculations obtained respectively using the MLAD and AHM PES's.

| | | | Observed | Obs−calc | | | |
|---|---|---|---|---|---|---|---|
| $\nu_1$ | $\nu_2$ | $\nu_3$ | G($\nu$) | M194 | MLAD | AW04 | AHM |
| 0 | 2 | 0 | 132.80 | 0.5 | 5.7 | 2.5 | 2.5 |
| 0 | 4 | 0 | 286.11 | -2.7 | -1.9 | -0.7 | -0.6 |
| 0 | 6 | 0 | 461.09 | -11.0 | -20.1 | 0.7 | 0.7 |
| 0 | 8 | 0 | 647.59 | -15.1 | -56.4 | -1.2 | -1.2 |

Continued on Next Page...

| | | | Observed | Obs−calc | | | |
|---|---|---|---|---|---|---|---|
| $\nu_1$ | $\nu_2$ | $\nu_3$ | G($\nu$) | [29] | MLAD | [13] | AHM |
| 0 | 10 | 0 | 848.40 | -19.1 | | -2.0 | -2.1 |
| 1 | 0 | 0 | 1224.20 | -5.3 | 1.9 | 5.2 | 5.1 |
| 1 | 2 | 0 | 1404.10 | -1.0 | 7.3 | 1.8 | -1.5 |
| 1 | 4 | 0 | 1590.05 | 0.1 | 3.4 | 0.1 | 0.1 |
| 0 | 18 | 0 | 1773.37 | | | -0.1 | -1.8 |
| 1 | 8 | 0 | 1990.52 | -6.6 | -43.6 | -3.4 | -3.5 |
| 0 | 0 | 1 | 2040.02 | 0.6 | 3.3 | 2.0 | 2.0 |
| 0 | 2 | 1 | 2133.89 | 4.7 | -3.0 | 0.1 | 0.1 |
| 1 | 10 | 0 | 2210.50 | -15.3 | | -0.7 | -0.9 |
| 2 | 0 | 0 | 2435.20 | -10.5 | 5.4 | 2.5 | 2.4 |
| 1 | 12 | 0 | 2439.90 | | | 1.4 | 1.0 |
| 0 | 24 | 0 | 2575.92 | | | -0.4 | 1.0 |
| 2 | 2 | 0 | 2656.33 | -3.9 | -15.3 | 0.4 | 0.3 |
| 2 | 4 | 0 | 2876.90 | -0.4 | 6.9 | 1.9 | 1.8 |
| 2 | 6 | 0 | 3099.90 | -1.6 | -3.6 | 3.3 | 3.1 |
| 1 | 0 | 1 | 3259.90 | | | 1.2 | 1.1 |
| 3 | 0 | 0 | 3636.10 | | | 0.1 | -0.1 |
| 3 | 2 | 0 | 3894.30 | | | -0.1 | -0.4 |
| 0 | 0 | 2 | 4035.37 | | | 0.4 | 0.1 |
| 0 | 2 | 2 | 4110.89 | | | 2.4 | 2.2 |
| 3 | 4 | 0 | 4146.30 | | | 2.5 | 2.2 |
| 0 | 4 | 2 | 4211.33 | | | 3.9 | 3.6 |
| 0 | 6 | 2 | 4339.42 | | | 5.1 | 4.6 |
| 3 | 6 | 0 | 4392.78 | | | 2.4 | 2.0 |
| 2 | 0 | 1 | 4459.30 | | | -0.8 | -1.2 |
| 3 | 8 | 0 | 4641.03 | | | 2.9 | 2.4 |
| 0 | 10 | 2 | 4651.60 | | | 3.4 | 2.3 |
| 0 | 12 | 2 | 4832.50 | | | 3.4 | 2.0 |
| 4 | 0 | 0 | 4828.70 | | | -1.3 | -1.9 |
| 0 | 14 | 2 | 5029.00 | | | 4.4 | -2.1 |
| 0 | 16 | 2 | 5236.60 | | | 4.1 | -2.0 |
| 1 | 0 | 2 | 5265.40 | | | -7.7 | -8.3 |
| 1 | 2 | 2 | 5367.20 | | | -7.1 | -8.0 |
| 1 | 4 | 2 | 5495.40 | | | -5.6 | -6.4 |

Continued on Next Page...

| | | | Observed | Obs−calc | | | |
|---|---|---|---|---|---|---|---|
| $\nu_1$ | $\nu_2$ | $\nu_3$ | G($\nu$) | [29] | MLAD | [13] | AHM |
| 1 | 6 | 2 | 5643.50 | | | -4.1 | -5.1 |
| 1 | 8 | 2 | 5809.10 | | | -2.4 | -4.0 |
| 5 | 0 | 0 | 6013.60 | | | -1.7 | -3.1 |
| 6 | 0 | 0 | 7191.30 | | | -0.9 | -4.8 |
| 7 | 0 | 0 | 8361.50 | | | 0.3 | -6.4 |

The calculations were performed up to energy levels of 12500 $cm^{-1}$ where a conical intersection Ahmed [13] with an electronic exited state PES forbid further calculations with the present method.

To reproduce the accurate spectra of cool stars atmosphere in the temperature range of $2000 - 4000$ K it is necessary perform calculations with a high rotational quantum number. Considering that the calculated and observed rotational constant is about $0.4cm^{-1}$ at an energy of 12000 $cm^{-1}$, $J$ should be approximately 86 (from equation 2.2.4). For this reason, energy levels with $J \gg 0$ have been tested. See Tables 3.1 for the MLAD and AHM1 PES and comparison with experimental data is shown. Both potential surfaces will need some adjustments and probably, a fit with experimental data could increase the accuracy of results.

### 3.1.2 Testing Procedure and Unexpected Levels

As we already said a potential energy surface represents the electronic potential energy field of a chemical bonded system for each geometric configuration of carbon nuclei.

This surface needs to cover all range of nuclear configurations without have regions or points in which the value of energy is unrealiable.

During the testing procedure to optimize DVR3D parameters, the AHM PES presented an unexpected and unreasonable behaviour. In particular, when

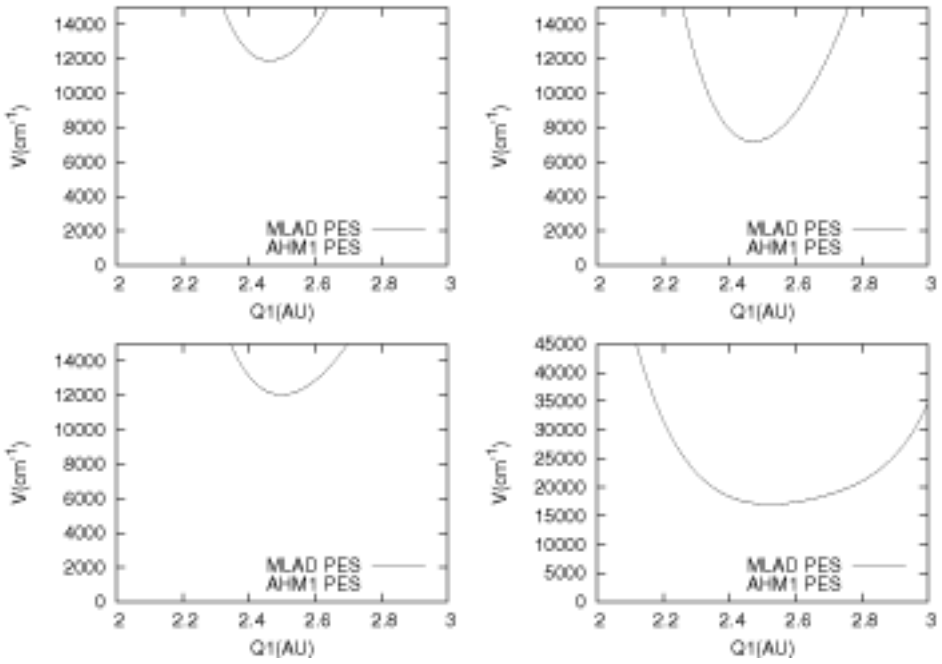


Figure 3.2: MLAD and AHM1 PESs as a function of the bondlength $q_1$.$\theta$ is fixed at 90 ° and $q_2$ from the left top assumes value 2.3, 2.45016, 2.7, 2.8 $a_0$ respectively

varying the values of the scattering coordinates $R$ and $r$ over certain values, unexpected lines are found to appear.

As we have already seen, the AHM potential energy surface is given in symmetric and antisymmetric stretch coordinates $X_1$, $X_2$ and $\theta$. A trasformation is therefore necessary to transform into Jacobi coordinates $r$, $R$ and $\alpha$ (coordinate system used in the DVR3D program).

A subroutine written in Fortran performs the transformation between the Bond-Length coordinates ($q_1$, $q_2$ and $\theta$) and the Jacobi coordinates (R, r, XCOS =cos($\alpha$)) using following relationships

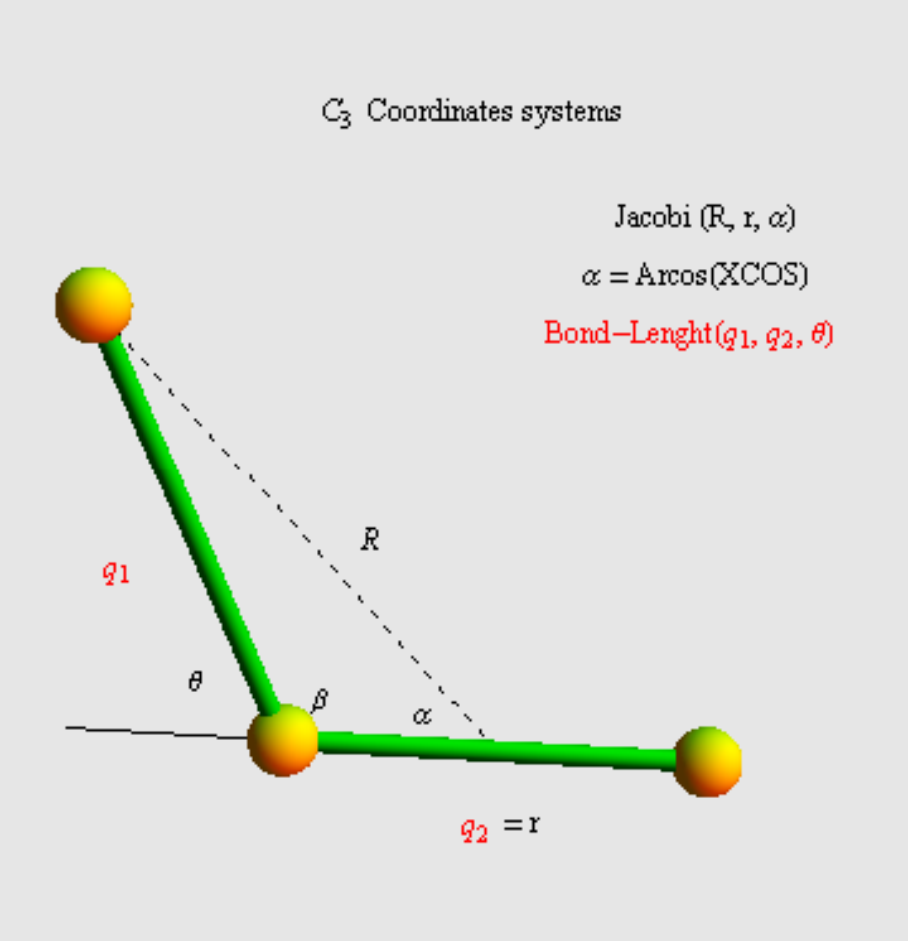


Figure 3.3: $C_3$ coordinate systems: Bond-Length and Jacobi

$$YY = \left(\frac{q_2}{2}\right) \tag{3.1.2}$$

$$R = r\left(\sqrt{q_1^2 - q_2}\cos(\beta)q_1 + \frac{q_2^2}{4}\right) \tag{3.1.3}$$

$$r = q_2 \tag{3.1.4}$$

$$XCOS = \frac{\frac{q_2^2}{2} - q_1 q_2 \cos(\beta)}{q_2\sqrt{q_1^2 - q_2\cos(\beta)q_1 + \frac{q_2^2}{4}}} \tag{3.1.5}$$

It seemed that over certain values the PES presented holes, that is points (or molecular configurations) for which it does not give realiable energy values.

It was necessary to make some adjustments to the AHM PES in order to use it within DVR3D. To calculate where the PES stopped working properly it was first necessary to perform a coordinate transformation to into Jacobi coordinates in order to have a comparable reference with AHM PES features (expressed in bond-lenght) and the results coming out running DVR3D. Deriving the expressions for ($q_1$, $q_2$ and $\theta$) from equation (3.1.2) it is possible rewrite the PES in Jacobi coordinates as follow (from equation 3.1.1)

$$V = \sum_{i,j,k} C_{i,j,k} J_1^i J_2^j J_3^k \tag{3.1.6}$$

where

$$J_1 = r_1 - 2r_e + \sqrt{\frac{{r_1}^2}{4} - r_2 \cos(\alpha) r_1 + {r_2}^2}, \tag{3.1.7}$$

$$J_2 = \sqrt{\frac{{r_1}^2}{4} - r_2 \cos(\alpha) r_1 + {r_2}^2} - r_1, \tag{3.1.8}$$

$$J_3 = \cos^{-1}\left( \frac{r_1 r_2 \cos(\alpha) - \frac{{r_1}^2}{2}}{r_1 \sqrt{\frac{{r_1}^2}{4} - r_2 \cos(\alpha) r_1 + {r_2}^2}} \right), \tag{3.1.9}$$

$C_3$ has a conical intersection at 12500 $cm^{-1}$ (Vlim) where energy levels calculations should be stopped on a single surface; this equilateral triangle configuration needs to be analysed and included as constraint for the PES expression. Introducing deformation coordinates make it easy to find out which conditions need to be added in order to constrain the PES to the region of interest. Deformation coordinates are defined as

$$S_1 = \frac{Q_1 + Q_2 + Q_3 - 3r}{\sqrt{3}}, \tag{3.1.10}$$

$$\begin{aligned}
S_2 &= \frac{Q_2 - Q_1}{\sqrt{2}}, && (3.1.11)\\
S_3 &= \frac{-Q_1 - Q_2 + 2Q_3}{\sqrt{6}}, && (3.1.12)\\
\tan\phi &= \frac{S_1}{S_2}, && (3.1.13)\\
&= \sqrt{3}\frac{Q_2 - Q_1}{-Q_1 - Q_2 + 2Q_3}, && (3.1.14)\\
\phi &= \tan^{-1}\left(\frac{\sqrt{3}(Q_2 - Q_1)}{-Q_1 - Q_2 + 2Q_3}\right), && (3.1.15)\\
S &= \sqrt{\frac{2}{3}}(Q_1 + Q_2 + Q_3), && (3.1.16)\\
Q_3 &= \sqrt{Q_1^2 + 2Q_2\cos(\theta)Q_1 + Q_2^2}, && (3.1.17)
\end{aligned}$$

Imposing equilateral configurations Q1=Q2=Q3 above equations become

$$S_1 = 3\frac{Q2 - r}{\sqrt{3}}, \tag{3.1.18}$$

$$\begin{aligned}
S_2 &= 0, && (3.1.19)\\
S_3 &= 0, && (3.1.20)\\
S &= \sqrt{\frac{2}{3}}3Q_2 = \sqrt{6}Q_2, && (3.1.21)
\end{aligned}$$

It was found that the conditions for $R < 2.6d0$ and $R < 2.0689d0*(r-1.55d0)$ correspond ignoring the region where the PES shows the holes see Figure 3.4. The line

$$R = 2.0689d0 * (r - 1.55d0), \tag{3.1.22}$$

was traced so is to cut the surface at the point beyond which the hole appears. The coefficients of the line where found through an empirical search varying them until the correct cut where visualized and obtained. The constraint $S_1 > 0.835703437d0$ is found from equation 3.1.24 this imposing the maximum value for $Q$ calculated using triangle rule with the fixed value $R = 2.6d0$.

All of these conditions need to be combined with the other constraint $xcos < 0.45d0$ corrisponding to the value where DVR3D stops calculating values for each angular grid-point.

A program was written with `Mathematica`™ [**?**] to produce a visual representation of the PES behaviour and developing the corrections. The `Mathematica`™ [**?**] program performs

- PES Coordinates transformation from Bond-Length to Jacobi coordinates and plots (see Figure 3.4) a representations of PES in Jacobi coordinates. This allows one to visualize the PES holes and the regions where critical values are encontered.
- contour plots of the surface Figure 3.5 fixing the range for $R$ and $r$ together with the lines such as Equation 3.1.22.

The following constraints were used in the Fortran subroutine to implement the constraints when running DVR3D to perform energy levels calculations:

$$\mathbf{IF}(S_1 > 0.835703437d0 \wedge xcos < 0.45d0) \Rightarrow V = V_{\text{Lim}} \quad (3.1.23)$$

$$\mathbf{IF}(R < 2.6d0 \wedge xcos < 0.45d0) \Rightarrow V = V_{\text{Lim}} \quad (3.1.24)$$

$$\mathbf{IF}(R < 2.0689d0 * (r1 - 1.55d0) \wedge xcos < 0.45d0) \Rightarrow V = V_{\text{Lim}} \quad (3.1.25)$$

Adding these constraints to the PES the problem of the appereance of unexpected lines was partially resolved as shown in Table 3.2.

Having constrained the PES to resolve the issue of unexpected lines in the spectra we must be aware that too many surface contraints could lead to problems in convergence. The issue of convergence is addressed in the next Section.

Table 3.2: Vibrational energy levels calculations performed by Ahmed *et al.* [13] are compared with DVR3D calculations obtained respectively using the AHM and Corrected AHM PES's.

| | | | Energy ($cm^{-1}$) | | |
|---|---|---|---|---|---|
| $\nu_1$ | $\nu_2$ | $\nu_3$ | AW04 [13] | AHM | Corr AHM |
| 0 | 0 | 0 | 0 | 0 | 0 |
| 0 | 2 | 0 | 137.99 | 137.97 | 137.97 |
| 0 | 4 | 0 | 294.51 | 294.46 | 294.46 |
| 0 | 6 | 0 | 468.09 | 468.08 | 468.08 |
| | | | | 653.73 | |
| 0 | 8 | 0 | 656.49 | 656.49 | 656.50 |
| 0 | 10 | 0 | 858.1 | 858.16 | 858.20 |
| 0 | 12 | 0 | 1072.06 | 1071.32 | 1072.27 |
| | | | | 1073.17 | |
| 1 | 0 | 0 | 1226.7 | 1226.77 | 1226.77 |
| 0 | 14 | 0 | 1297.43 | 1296.70 | 1298.22 |
| 1 | 2 | 0 | 1410 | 1410.08 | 1410.08 |
| | | | | 1483.92 | |
| 0 | 16 | 0 | 1533.97 | 1537.59 | 1535.07 |
| 1 | 4 | 0 | 1597.65 | 1597.66 | 1597.67 |
| 0 | 18 | 0 | 1781.17 | 1764.15 | 1775.14 |
| 1 | 6 | 0 | 1794.51 | 1794.59 | 1794.59 |
| | | | 1915.63 | | 1978.3 |
| 1 | 8 | 0 | 2001.62 | 2001.73 | 2001.73 |
| 0 | 20 | 0 | 2038.79 | | |
| 0 | 0 | 1 | 2045.72 | 2045.68 | 2045.69 |
| | | | | 2079.16 | |
| 0 | 2 | 1 | 2141.49 | 2141.49 | 2141.49 |
| | | | | 2158.80 | |
| 1 | 10 | 0 | 2218.9 | 2219.03 | 2219.07 |
| | | | | 2235.25 | |
| 0 | 4 | 1 | | 2268.92 | 2268.92 |
| 0 | 22 | 0 | 2306.43 | 2315.56 | 2411.92 |
| 0 | 6 | 1 | | 2418.38 | 2418.40 |
| 2 | 0 | 0 | 2440.4 | 2440.514 | 2440.52 |
| 1 | 12 | 0 | 2446.2 | 2446.24 | 2446.63 |
| | | | | 2472.79 | |
| 0 | 24 | 0 | | 2584.02 | 2521.45 |

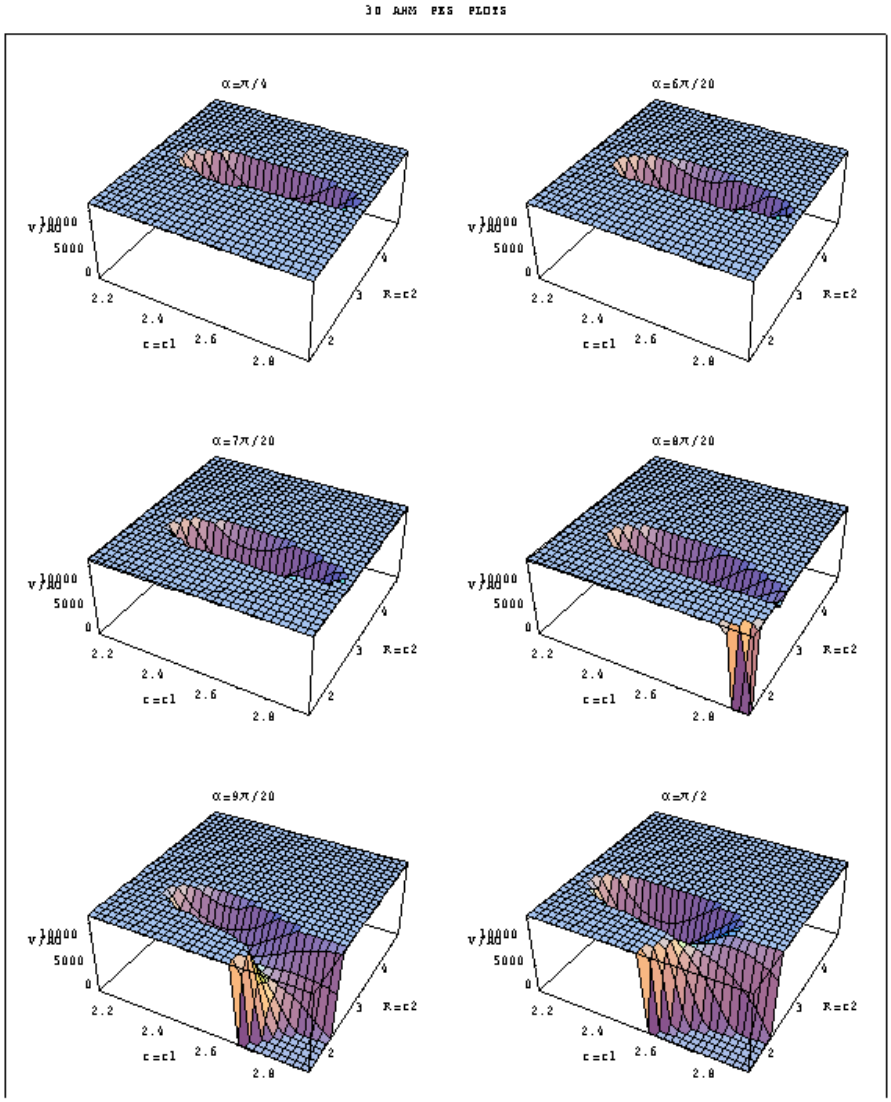


Figure 3.4: 3D Plots for AHM PES expressed in Jacobi coordinates fixing the $\alpha$ at values $(\pi/4, 6\pi/20, 7\pi/20, 8\pi/20, 9\pi/20, \pi/2))$

### 3.1.3 Convergence Tests

#### Definition of Convergence

Convergence describes the tendency of a quantity towards a certain value and in this particular case sets the accuracy of energy levels calculations.

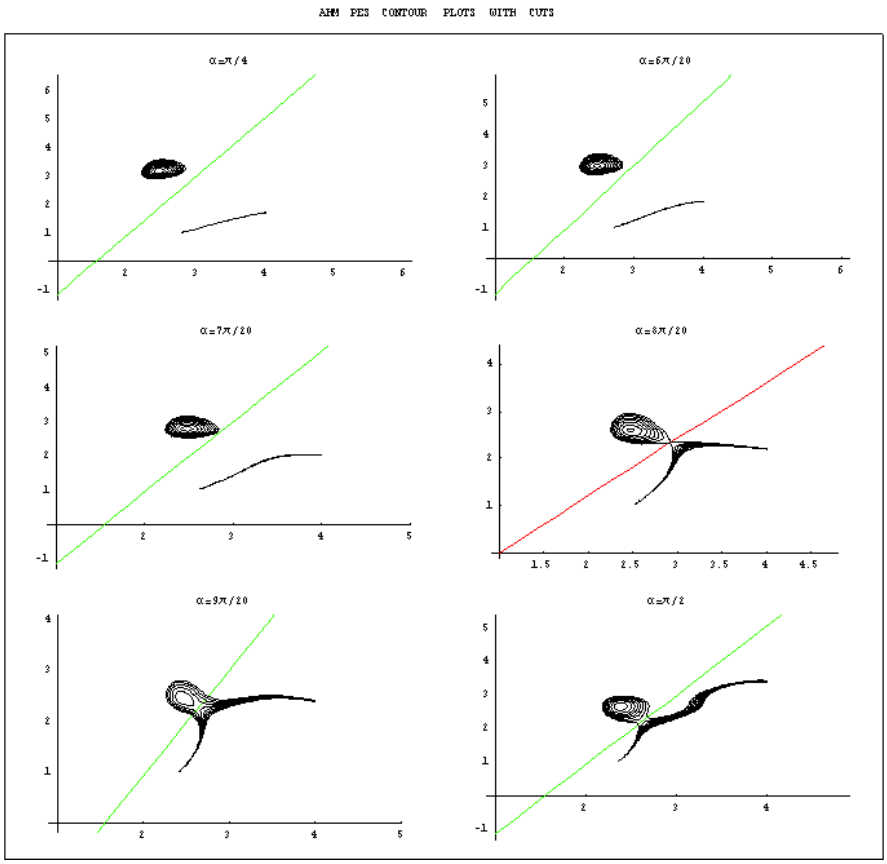


Figure 3.5: Countour plots in Jacobi coordinates fixing the $\alpha$ at values $(\pi/4, 6\pi/20, 7\pi/20, 8\pi/20, 9\pi/20, \pi/2)$ and line equation used to cut the potential energy surface to ignore holes.

Energy levels convergence need to be achieved finding optimal value for the DVR3D parameters. A compromise between accuracy and computational time need to be taken in consideration when in DVR3D radial and angular points are choosen and when the dimensions of the vibrational and rotational problem is set.

**Testing Proceedure**

Convergence tests for the pure vibrational problem were performed for $J = 0$. Parameters were choosen in order to perform a correct description of the molecular system using DVR3D as computational theoretical tool. DVR3D requires as input a file with 9 lines in which all the settings can be specified [1].

- **NPNT1/NPNT2** number of DVR points in R/r from Gauss-(associated) Laguerre quadrature.
- **NALF** number of DVR points in $\theta$ from Gauss-(associated) Legendre quadrature.
- **MAX3D** maximum dimension of the final Hamiltonian.
- **EMAX2** is the second cut-off energy in $cm^{-1}$ with the same energy zero as the potential.
- **ZCUT= True** final dimension selected using an energy cut-off given by EMAX2.
- **ZCUT= False** final dimention determined by MAX3D.

The number of radial and angular points and the Hamiltonian dimension were choosen setting initial values considering specific properties of the molecule and its PES, and then iteratively optimized.

**First step** Radial numbers (NPNT1, NPNT2) optimization.

- Morse oscillator parameter ($r_e$, we, De) varied until stability of energy levels results are demostrated.
- fixing Morse parameters, NPNT are varied until the energy levels difference between previous and successive calculations are at the accuracy order of 0.01 $cm^{-1}$.

**Second step** Number of angular functions (NALF) and Hamiltonian dimention optimization.

- Setting values for $ZCUT = False$, $NALF = 80$ and $MAX3D = 2000$ (these is setted looking to previous calculation experiences) the calculation output will give a value for the Energy in wavenumber $E^*$.
- Test with values $ZCUT = True$, $NALF = 90$, $MAX3D = 3000$ and $Emax3D = E^*$ energy levels stability.

Then optimal values for: $r_e$, we, De should be found for both radial and Jacobi coordinates.

**Results**

The final optimized value are:

- Radial number of points for $R = 56$, for $r = 26$ and the angle is $\alpha = 80$.
- Hamiltionian dimension is 2000.
- Morse oscillators optimized parameters expressed in a.u. are
  - $r_e = 3.675$, $\text{we}_1 = 0.005$, $\text{De}_1 = 0.3$
  - $r_e = 2.585$, $\text{we}_2 = 0.010$, $\text{De}_2 = 0.3$.

**Issues and Futher Work**

An important parameter to determine is the size of the Hamiltonian in the rotation module (see value ROTLEV3). This value (IBASS) was partially determinated but futher tests are necessary.

Tests were also done for several quantum numbers $J$. When looking at large $J$, a problem was encontered with the program used to perfom the calculations.

Early test results for $J = 20$ shows a that the possible valuefor IBASS has to be greather than 750. Further tests to find a value for IBASS are necessary with J at least larger then 40.

## 3.2 Dipole Moment Surface

The second thing needed to calculate a line-list is a reliable Dipole Moment Surface (DMS).

### 3.2.1 Constuction of a DMS

As described for the PES, aDMS is built by interpolating ab-initio dipole moment components estimated for each nuclear geometric configuration using appropriate functional forms. The $C_3$ molecule has no permanent dipole moment but the diplacements from the equilibrium induce a dipole moment components.

#### Comparison of ab-initio and Fitted Dipole Moment Surface for $C_3$

If a working DMS is already available, one can compute transition intensities without performing ab-initio calculations and interpolation. In the case of $C_3$, ab-initio dipole moment calculations for $C_3$ molecule are already available. These are kindly provided by Colin Western, School of Chemistry, University of Bristol. The 587 ab-initio points (for each component) were calculated by Ahmed at al. [13] (AHM2) using MRCI (Multi-Reference Configuration Iteration) method with the MORPLO Package [27].

Despite the availability of ab-initio dipole surfaces for $C_3$ previously constructed by Jorgensen *et al.*. [32] (JORG) and Jensen *et al.*. [18] (JENS), we decide to built a new DMS due to the higher quality of AHM ab-initio calculations for reason explained below.

### 3.2.2 The Jorgensen and Jensen DMS

The surfaces of Jorgensen [32] were obtained to an accuracy sufficient for the astrophysical predictions their work required. It will not be tested here but these results have been compared with my calculations see table 3.4 and 3.5. While Jorgensen placed less emphasis on describing the properties of the

molecule near equilibrium geometry, Jensen *et al.*. [18] focused their study instead on the behavior near the equilibrium configuration.

The JENS DMSs were tested and comparisons made to test the new DMS. The JENS DMS was constructed by fitting the $p$ and $q$ molecular dipole moment components (see Figure 3.6 where axes x and z represent p and q axes) for $\theta$ between $180\,^\circ$ (linear) and $90\,^\circ$ and bond lengths from 1.16 to 1.43 $\mathring{A}$. Dipole moments was calculated using the MOLECULE-SWEDEN code [33].

Employing a complete-active space self-consistent field (CASSCF) method which uses the full valence space. A second calculation step could be performed selecting some of the CASSCF values and perform caculations at Multi-reference configuration iteration levels considering also furthe configuration interaction (CI) effects. The MRCI values are more difficult to estimate and they require more computer time; this is the reason why just CASSCF values may be used. Despite the higher accuracy of MRCI calculations the smaller number of nucler configurations used could lead to some problems during the fitting procedure for builting the surface. CASSCF values were used in the JENS final fit because of an insufficient numerical stability of the Multi-reference configuration iteration (MRCI) calculations. For this reason, and because of the larger AHM ab-initio grid points range, we believe that the AHM MRCI ab-initio calculations should be used instead.

### 3.2.3 A New Formulation of the DMS

AHM's functions were calculated for $\theta$ between $180\,^\circ$ (linear) and $60\,^\circ$ (equilateral triangle geometry) and bond lengths ranging from 0.4 $\mathring{A}$ to $= 1.29497\mathring{A}$.

AHM ab-initio points were fitted using a functional form proposed by Partridge and Schwenke(PS) [28] to study the water problem. It has been necessary perform a coordinates transformation between the coordinates reference system used by AHM and the one used by Partridge. The carbon atoms are set in the xz plan with the central atoms at the origin of the system and the remaining atoms having coordinates atom 1 $x = q_1 \cos(\frac{\theta}{2})$, $z = q_1 \sin(\frac{\theta}{2})$ and atom 2 $x = q_2 \cos(\frac{\theta}{2})$ , $z = -q_2 \sin(\frac{\theta}{2})$. The coordinate systems are shown in

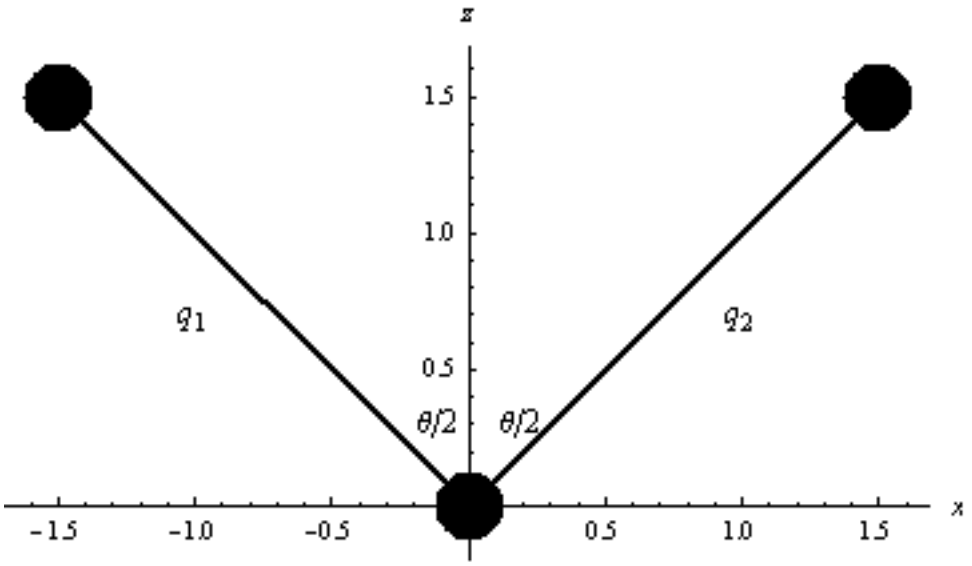


Figure 3.6: Partridge and Schwenke(PS) [28] coordinates system $C_3$.

Figure 3.6.

### 1) The PS Function

The choise of the dipole moment functional form is important to describe the correct behaviour.

The PS function is given by

$$\begin{aligned} \vec{\mu}\left(q_2, q_1, \theta\right) &= q\left(q_1, q_2, \theta\right)\left(\vec{x_{\mathrm{C1}}} - \vec{x_{\mathrm{C2}}}\right) + \\ &\quad + q\left(q_2, q_1, \theta\right)\left(\vec{x_{\mathrm{C3}}} - \vec{x_{\mathrm{C2}}}\right) \end{aligned} \tag{3.2.1}$$

with

$$
\begin{aligned}
q\left(q_1, q_2, \theta\right) &= \exp(-\beta(q_1 - r_e)^2)\left(\sum_{i=1}^{\mathrm{nr}} \mathrm{C}_i \left(\frac{\mathrm{q}_{2-r_e}}{r_e}\right)^i\right) \\
&\quad + \exp(-\beta q_1 - r_e)^2) \sum_{ijk} \mathrm{C}_{ijk} \left(\frac{q_2 - r_e}{re}\right)^i \left(\frac{q_2 - r_e}{r_e}\right)^j \\
&\quad \times \left(\cos\theta - \cos\theta_e\right)^k \qquad (3.2.2)
\end{aligned}
$$

with the second sum having:

$$
\begin{aligned}
i + j + k &\leq n_\theta, \qquad (3.2.3) \\
j + k &> 0, \qquad (3.2.4) \\
i + j &\leq n_r, \qquad (3.2.5) \\
n_r &\leq n_\theta \qquad (3.2.6)
\end{aligned}
$$

The PS function is controlled by two terms $n_r$ and $n_\theta$ and their value is limited by the number of radial and angular number of points. The non -linear parameters $\beta$ was fixed equal to $2a_0^{-2}$ and the parameters $\mathrm{C}_{ijk}$ $\mathrm{C}_i$ are calculated using a linear last-squares fit. The fit was obtained for $q$ using a Mathematica program written by Lorenzo Lodi (UCL). This is set out in Table 3.3.

During the fitting procedure some points has been added to constain behaviour in equilateral triangle configurations where a zero dipole moment is expected by symmetry. Increasing the number of parameters results in a fit which shows oscillations see Figure 3.7. The final fit chosen has $n_\theta = 7$ and $n_r = 4$, Table 3.3 gives the results. The values used for $r_e$ is 2.46 a.u and $\theta_e$ corresponds to the linear configuration.

Table 3.3: AHMPS Fit parameters in a.u, with $n_r = 4$, $n_\theta = 7$ and $\beta = 3.7$

| i | j | k | q | i | j | k | q |
|---|---|---|---|---|---|---|---|
| 0 | 0 | 0 | -0.1854 | 1 | 1 | 0 | 0.0467 |
| 1 | 0 | 0 | 1.0897 | 1 | 1 | 1 | 15.0394 |
| 2 | 0 | 0 | -6.1417 | 1 | 1 | 2 | -102.5349 |
| 3 | 0 | 0 | 28.6315 | 1 | 1 | 3 | 224.6806 |
| 4 | 0 | 0 | -31.7287 | 1 | 1 | 4 | -190.0721 |
| 0 | 0 | 1 | 0.1920 | 1 | 1 | 5 | 53.2123 |
| 0 | 0 | 2 | -1.4374 | 1 | 2 | 0 | 4.5036 |
| 0 | 0 | 3 | 7.4693 | 1 | 2 | 1 | -177.7461 |
| 0 | 0 | 4 | -17.7946 | 1 | 2 | 2 | 712.8167 |
| 0 | 0 | 5 | 20.8125 | 1 | 2 | 3 | -935.1822 |
| 0 | 0 | 6 | -11.8490 | 1 | 2 | 4 | 387.0837 |
| 0 | 0 | 7 | 2.6297 | 1 | 3 | 0 | 8.2939 |
| 0 | 1 | 0 | -0.2030 | 1 | 3 | 1 | -67.2054 |
| 0 | 1 | 1 | -1.4017 | 1 | 3 | 2 | -61.9312 |
| 0 | 1 | 2 | 10.8417 | 1 | 3 | 3 | 71.1487 |
| 0 | 1 | 3 | -31.3581 | 2 | 0 | 1 | -3.5201 |
| 0 | 1 | 4 | 42.5052 | 2 | 0 | 2 | 64.7173 |
| 0 | 1 | 5 | -28.4328 | 2 | 0 | 3 | -172.0531 |
| 0 | 1 | 6 | 7.7838 | 2 | 0 | 4 | 158.1754 |
| 0 | 2 | 0 | 0.4010 | 2 | 0 | 5 | -46.1796 |
| 0 | 2 | 1 | 11.7281 | 2 | 1 | 0 | -12.0753 |
| 0 | 2 | 2 | -59.9290 | 2 | 1 | 1 | 93.3593 |
| 0 | 2 | 3 | 123.2878 | 2 | 1 | 2 | -367.7184 |
| 0 | 2 | 4 | -104.7863 | 2 | 1 | 3 | 492.3506 |
| 0 | 2 | 5 | 30.5536 | 2 | 1 | 4 | -207.8296 |
| 0 | 3 | 0 | -3.9754 | 2 | 2 | 0 | -6.0008 |
| 0 | 3 | 1 | -42.3832 | 2 | 2 | 1 | -74.5952 |
| 0 | 3 | 2 | 108.2957 | 2 | 2 | 2 | 361.8279 |
| 0 | 3 | 3 | -90.6804 | 2 | 2 | 3 | -239.6715 |
| 0 | 3 | 4 | 24.3682 | 3 | 0 | 1 | -28.6117 |
| 0 | 4 | 0 | -23.7117 | 3 | 0 | 2 | 118.5863 |
| 0 | 4 | 1 | 234.0460 | 3 | 0 | 3 | -168.7359 |

Continued on Next Page...

| i | j | k | q | i | j | k | q |
|---|---|---|---|---|---|---|---|
| 0 | 4 | 2 | -387.7413 | 3 | 0 | 4 | 67.9076 |
| 0 | 4 | 3 | 174.0015 | 3 | 1 | 0 | 34.6425 |
| 1 | 0 | 1 | 0.5393 | 3 | 1 | 1 | -336.1718 |
| 1 | 0 | 2 | -7.2829 | 3 | 1 | 2 | 474.0681 |
| 1 | 0 | 3 | 19.9636 | 3 | 1 | 3 | -217.1211 |
| 1 | 0 | 4 | -25.0169 | 4 | 0 | 1 | -91.5287 |
| 1 | 0 | 5 | 16.7842 | 4 | 0 | 2 | 290.5264 |
| 1 | 0 | 6 | -5.0748 | 4 | 0 | 3 | -164.9791 |

### 3.2.4 Comparison of DMSs

Having constructed a DMS we are faced with the problem of evaluating how good it is. In order to choose a good DMS we need to perform tests and make comparisons between all data available. The problem is that there are not many experimental or observational absolute intensity measurements. The data available are due to Treffers and Gilda [34], Kramer and Jorgesen [32]and Jensen *et al.*. [18].

A program to calculate dipole transition intensities, DIPOLE3, is available as part of the DVR3DRJ package [1].

Vibrational transition moments reported by Jensen [18] were comparated with values obtained using DIPJ0DVR [35]. This program needs as input an accurate and smooth DMS to perform detailed investigations.

Comparison between previous calculations and the new one are shown in Table 3.4.

The AHM DMS shows a good agreement with all data available and this is the one I recomend using to perform the $C_3$ transition intensity calculations. Details about the fit can be found in file C3DIPOLE.

In Conclusion, a wide overview of $C_3$ molecular system and all preparatory

| Energy ($cm^{-1}$) | | $\nu_1$ | $\nu_2$ | l | $\nu_3$ | $\nu_1'$ | $\nu_2'$ | l' | $\nu_3'$ | [18] | [34] | [32] |
|---|---|---|---|---|---|---|---|---|---|---|---|---|
| Bra | Ket | Bra | | | | Ket | | | | | | |
| 0.85 | 0.00 | 0 | 0 | 1 | 0 | 0 | 0 | 0 | 0 | | 0.0508 | 0.0384 |
| 68.00 | 0.00 | 0 | 1 | 1 | 0 | 0 | 0 | 0 | 0 | 0.4371 | 0.3915 | 0.4115 |
| 214.70 | 0.00 | 0 | 3 | 1 | 0 | 0 | 0 | 0 | 0 | 0.0131 | 0.0241 | 0.0291 |
| 137.90 | 68.00 | 0 | 2 | 0 | 0 | 0 | 1 | 1 | 0 | 0.3513 | 0.3401 | 0.3529 |
| 295.30 | 68.00 | 0 | 4 | 0 | 0 | 0 | 1 | 1 | 0 | 0.0185 | 0.0272 | 0.0288 |
| 469.03 | 68.00 | 0 | 6 | 0 | 0 | 0 | 1 | 1 | 0 | 0.0020 | 0.0004 | 0.0041 |
| 214.70 | 137.90 | 0 | 3 | 1 | 0 | 0 | 2 | 0 | 0 | 0.4902 | 0.4528 | 0.4735 |
| 380.13 | 137.90 | 0 | 5 | 1 | 0 | 0 | 2 | 0 | 0 | 0.0288 | 0.0422 | 0.0424 |
| 561.40 | 137.90 | 0 | 7 | 1 | 0 | 0 | 2 | 0 | 0 | 0.0041 | 0.0034 | 0.0067 |
| 1320.47 | 0.00 | 1 | 1 | 1 | 0 | 0 | 0 | 0 | 0 | 0.0167 | 0.0195 | 0.0050 |
| 1504.41 | 0.00 | 1 | 3 | 1 | 0 | 0 | 0 | 0 | 0 | 0.0022 | 0.0050 | 0.0027 |
| 1226.70 | 68.00 | 1 | 0 | 0 | 0 | 0 | 1 | 1 | 0 | 0.0167 | 0.0122 | 0.0005 |
| 1410.00 | 68.00 | 1 | 2 | 0 | 0 | 0 | 1 | 1 | 0 | 0.0165 | 0.0224 | 0.0075 |
| 1597.65 | 68.00 | 1 | 4 | 0 | 0 | 0 | 1 | 1 | 0 | 0.0016 | 0.0067 | 0.0034 |
| 1320.00 | 137.90 | 1 | 1 | 1 | 0 | 0 | 2 | 0 | 0 | 0.0165 | 0.0110 | 0.0017 |
| 1504.41 | 137.90 | 1 | 3 | 1 | 0 | 0 | 2 | 0 | 0 | 0.0230 | 0.0308 | 0.0110 |
| 1696.23 | 137.90 | 1 | 5 | 1 | 0 | 0 | 2 | 0 | 0 | 0.0210 | 0.0093 | 0.0049 |

Table 3.4: Our DIPJ0 calculations obtained using the AHMDMS are compared with calculations performed by: Jensen [18] and Jorgesen [32]

| Energy ($cm^1$) | | $\nu_1$ | $\nu_2$ | $l$ | $\nu_3$ | $\nu_1'$ | $\nu_2'$ | $l'$ | $\nu_3'$ | [18] | AHMPART | [34] | [32] |
|---|---|---|---|---|---|---|---|---|---|---|---|---|---|
| Bra | Ket | Bra | | | | Ket | | | | | | | |
| 0.00 | 0.00 | 0 | 0 | 0 | 0 | 0 | 0 | 0 | 0 | | 0.0491 | | |
| 2045.72 | 0.00 | 0 | 0 | 0 | 1 | 0 | 0 | 0 | 0 | 0.3460 | 0.3198 | 0.2209 | 0.3202 |
| 2141.49 | 0.00 | 0 | 2 | 0 | 1 | 0 | 0 | 0 | 0 | 0.0112 | 0.0961 | | |
| 2045.72 | 137.90 | 0 | 0 | 0 | 1 | 0 | 2 | 0 | 0 | 0.0112 | 0.0623 | | |
| 2141.49 | 137.90 | 0 | 2 | 0 | 1 | 0 | 2 | 0 | 0 | 0.3320 | 0.2773 | | |
| 2268.92 | 137.90 | 0 | 4 | 0 | 1 | 0 | 2 | 0 | 0 | 0.0155 | 0.1145 | | |
| 2418.37 | 137.90 | 0 | 6 | 0 | 1 | 0 | 2 | 0 | 0 | 0.0014 | 0.0240 | | |
| 3266.00 | 0.00 | 1 | 0 | 0 | 1 | 0 | 0 | 0 | 0 | | 0.0459 | 0.0552 | 0.0194 |

Table 3.5: Transition moments in Debye. Calculations performed by Jensen et al. [18] are compared with our DIPJ0 calculations obtained using the AHMDMS, Jorgesen calculations [32] and with experimental values obtained by Treffers [34].

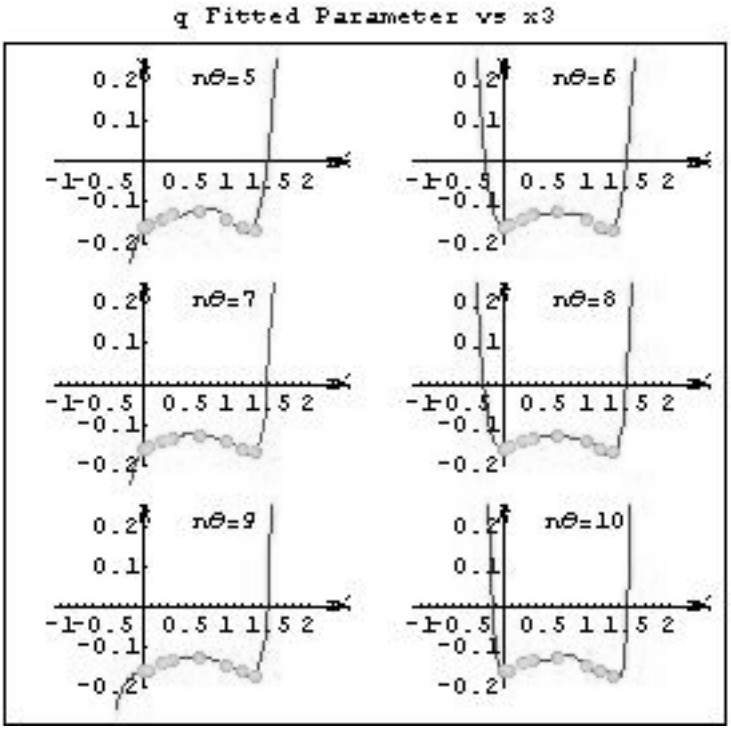


Figure 3.7: Oscillations in AHMDMS fit with increasing number of angular points.

work for linelist calculation have been decribed. Future work will involve performing other necessary tests and starting the actual calculations to complete this lineslist computational project.

# Chapter 4

# Conclusion

## 4.1 Summary

In Conclusion, a wide overview of $C_3$ molecular system and all preparatory work for linelist calculation have been described.

## 4.2 Future Work

Future work will involve performing other necessary tests and starting the actual calculations to complete this lineslist computational project. First, it will be necessary testing and choose the value for IBASS as explained in the last section. This is the only parameter left to test in DVR3D before to start performing energy level calculations. An unformatted file printed out running ROTLEV is used from DIPOLE module to perform transition intensity calculations. The parameter to set in DIPOLE are the number of eigenfunctions considered and the ground state relative to the energy zero [1]. Calculation of a number of energy levels large enough allows to use the Boltzman statistics to determine partition functions. It is the module SPECTRA in DVR3D that allows to perform those calculations. Opacity value for $C_3$ could let a better modelling of atmospheric dynamics in those stars were $C_3$ molecules aboundancy plays an important role. I hope the

preparatory work explained in this report could support the future work.

# References


[1] J. Tennyson et al. DVR3D: a program suite for the calculation of rotation-vibration spectra of triatomic molecules. *Comput. Phys. Commun.*, 163:85–116, 2004.

[2] U. G Jorgesen. *Rev. Mexicana Astron. Astrf.*, 23:49–62, 1992.

[3] A. Braccesi. *Dalle stelle all'universo, lezioni di Astrofisica*. Zanichelli, 2000.

[4] W. Weltner and R. J. Van Zee. Carbon molecules, ions, and clusters. *Chem. Rev.*, 89:1713–1747, 1989.

[5] J.R. Goicoechea and J. Cernicharo. Spectroscopy of key molecular species in the infrared. *ApJ*, 2001.

[6] B. T. Sutcliffe and J. Tennyson. *Internat. J. Quantum Chem.*, 39:183–196, 1991.

[7] P. R. Bunker. Quasiliner and quasiplanar molecule. *Ann. Rev. Phys. Chem.*, 1983.

[8] W. P. Kraemer. A theoretical study of the rotation-vibration energy levels and dipole moment functions of $CCN^+$, $CNC^+$ and $C_3$. *J. Mol. Spectrosc.*, 107:191–207, 1984.

[9] D. H. Liskow, C. F. Bender, and H. F. Schaefer. *J. Chem. Phys.*, 1972.

[10] F. J. Northrup and T. J. Sears. Stimulated-emission pumping spectrocscopy study of jet-cooled $C_3$: pure bending levels and bend-symmetric combination levels of $\widetilde{X}\Sigma_g^+$. *J. Opt. Soc. Am.*, 7:1924–1933, 1990.

[11] E. A Rohlfing and J. E. M. Goldsmith. Stimulated-emission pumping spectroscopy of jet-cooled $C_3$: antisymmetric stretch-bent levels. *J. Opt. Soc. Am.*, 7:1915–1923, 1990.

[12] F. J. Northrup, T. J. Sears, and E. A. Rohlfing. A semirigid bender analysis of an extensive set of rotation-vibration levels in $\widetilde{X}\Sigma_g^+$ of $C_3$. *J. Mol. Spectrosc.*, 145:74–88, 1991.

[13] K. G. Ahmed, G. Balint-Kurti, and C. M. Western. Ab initio calculations and vibrational energy level fits for the lower singlet potential-energy surfaces of $C_3$. *J. Chem. Phys*, 121:10041, 2004.

[14] F. J. Northrup and T. J. Sears. Observation ofstimulated emission pumping spectra of jet-cooled $C_3$. *Chem. Phys. Lett.*, 159:421–425, 1989.

[15] E. A. Rohlfing and J. E. M. Goldsmith. Stimulated-emission pumping spectroscopy of jet-cooled $C_3$. *J. Chem. Phys.*, 90:6804, 1989.

[16] G. Duxbury. *Infrared Vibation-Rotation Spectroscopy.* John Wiley and Sons, 2000.

[17] C. A. Schmuttenmaer, R. C. Cohen, N. Pugliano, J. R. Heath, A. L. Cooksy, K. L. Busarow, and R. J. Saykally. Tunable far-ir laser spectroscopy of jet-cooled carbon clusters: The $\nu_2$ bending vibration of $C_3$. *Science*, 249:897–900, 1990.

[18] P. Jensen, C. Rohlfing, and J. Almof. Calculation of the complete-active-space self-consistent-field potential-energy-surface, the dipole moment surfaces, the rotation-vibration energies, and the vibrational transition moments for $C_3$. *J. Chem. Phys.*, 97:3399, 1992.

[19] G. Zhang, K. S. Chen, A. J. Merer, Y. C. Hsu, W. J. Chen, S. Shaji, and Y. A. Liao. The 4051-$a$ band of $C_3$:perturbated low-j lines and life time measurament. *J. Chem. Phys.*, 122:1–8, 2005.

[20] A. D. Walsh. *Discuss. Farday Soc.*, 35, 1963.

[21] J. J. Keady et al. The IRC+10216 circumstellar envelope models forthe dust and gas. *ApJ*, 326:832–842, 1988.

[22] K. W. Hinkle, J. J. Keady, and P. B. Bernath. Detenction of $C_3$ in the circumstellar shell of irc+10216. *Science*, 242:1319–1322, 1988.

[23] J. Cernicharo and J. R. Goicoechea. Far-infrared detection of $C_3$ in sagittarius B2 and IRC+10216. *ApJ*, 534:199–202, 2000.

[24] G. J. Harris, J. Tennyson, B. M. Kaminski, Ya. V. Pavlenco, and H. R. A. Jones. Improved HCN/HNC linelist, model atmospheres and synthetic spectra for WZ Cas. $Mon.Not.R.Astron.Soc., InPress$, 2006.

[25] P. Jensen and P. R. Bunker. *Computational molecular Spectroscopy*. John Wiley and Sons, 2000.

[26] O. L. Polyansky, A. G Csszr, Shirin S. V., Zobov N. F., P. Barletta, J. Tennyson, D. W. Schwenke, and Knowles P. J. High-accuracy ab initio rotation-vibratio transitions for water. *Science*, 299:539–542, 2003.

[27] J. Werner and P.J. Knowles. MORPLO, a package of ab-initio programs. 2002.

[28] H. Partridge and D. W. Schwenke. The determination of accurate isotope potential anergy surface for water from extensive ab initio calculations and experimental data. *J. Chem. Phys.*, 106:4618, 1997.

[29] M. Mladenovic, S. Schmatz, and P. Botschwina. Large-scale ab initio calculations for $C_3$. *J. Chem. Phys*, 101:5891, 1994.

[30] K. Kawaguchi, K. Matsumura, H. Kanamori, and E. Hirota. Diode laser spectroscopy of $C_3$: The $\nu_2 + \nu_3 - \nu_2$, $2\nu_2 + \nu_3 - 2\nu_2$ and $2\nu_2 + \nu_3$ bands. *J. Chem. Phys.*, 91:1953–1957, 1989.

[31] J. Baker. Observation of new bands in the lasr induced fluorescence spectrum of $C_3$. *J. Mol. Spectrosc.*, 183:6–11, 1997.

[32] U. G. Jorgesen, J. Almlof, P. Siegbahn, and M. F. Affiliation. *ApJ*, 343:554–561, 1989.

[33] J. Almof, C. W. Bauschlicher, P. E. M. Siegbahn, B. O. Roos, A. Heinberg, P. R. Taylor, Malmqvist P. A., and Rendell A. P. MOLECULAR SWEDEN.

[34] R. R. Trefferes and D. P. Girla. *Ap.J.*, 202, 1975.

[35] J. R. Henderson, C. R. Le Suer, and J. Tennyson. DVR3D:programs for fully pointwise calculation of vibrational spectra. 2006.

[36] B.J. McCall, R.N. Casaes, M. Adamkovics, and R.J. Saykally. A re-examination of the 4051 $\mathring{A}$ band of $C_3$ using cavity ringdown spectroscopy of a supersonic plasma. *Chem. Phys. Lett.*, 374:583–586, 2003.

[37] A. Tanabashi, T. Hirao, and T. Amano. Fourier trasform emission spectra of the (000)-(000) band of the 4051.6 $\mathring{A}$ band of $C_3$. *ApJ*, 624:1116–1120, 2005.

[38] J. Szczepanski, S. Ekern, and M. Vala. Vibrational spectroscopy of small matrix-isolated linear carbon cluster anions. *J. Phys. Chem.*, 101:1841–1847, 1997.

[39] J. Szczepanski, H. Wang, and M. Vala. Reaction of the $C_3$ carbon cluster with benzene. *Chem. Phys.*, 303:165–177, 2003.

[40] E. A. Rohlfing. Laser-induced-fluorescence spectrroscopy of jet-cooled $C_3$. *J. Chem. Phys.*, 91:6804, 1989.

[41] D. W. Schwenke and H. Partridge. Convergence testing of analytic representation of ab initio dipole moment function for water: Improved fitting yields improved intensities. *J. Chem. Phys.*, 113:6592–6597, 2000.

[42] V. Spirko and P. Jensen. Calculation of rotation-vibration energy levels in ground state $C_3$ by born-oppenheimer-type separation of the vibrational motions. *J. Mol. Spectrosc.*, 183:128–138, 1997.

[43] I. Plesser and Z. Vager. Structure of $C_3$ as measured by the Coulomb-Explosion technique. *Phys. Rev. Lett.*, 56:1559, 1986.

[44] R. Loidl, J. Hron, U. G. Jorgens, and S. Hofner. Proibing the outer atmosphere of carbon stars. $C_2$, $H_2$, HCN and $C_3$ features in the SWS range. *AA*, 56:1559, 1986.

[45] L. Gausset, G. Herzberg, A. Lagerqvist, and B. Rosen. *ApJ*, 142, 1965.

[46] O. Takeshi, J. A. Thorburn, B. J. McCall, S. D. Friedman, L. M Hobbs, P. Sonnentrucker, D. E Welty, and D. G York. Observations of $C_3$ in translucent slight light. *ApJ*, 582:823–829, 2003.

[47] T. F. Giensen, A. O. Van Orden, J. D. Cruzan, R. A. Provencal, R. J. Saykally, R. Gendriech, F. Lewen, and G. Winnewisser. *Ap. J. Lett.*, 555, 2001.

[48] R. Gendriech, T. F. Giensen, F. Lewen, and G. Winnewisser. Terahertz spectroscopy of linear triatomic ccc: High precision laboratory measurament and analysis of the ro-vibrational bending transitions. *Z.Naturforsch.*, 58a:129–138, 2003.

[49] A. E. Lynas-Gray, S. Miller, and J. Tennyson. Infrared transition intensities for water: A comparison of ab initio and fitted dipole moment surfaces. *J. Mol. Spectrosc.*, pages 458–467, 1995.

[50] R. G. LittleJohn, K. Mitchell, V. Aquilanti, and S. Cavalli. Body frames and frame singularities for three-atom systems. *Phys. Rev. A*, 58:3705–3717, 1998.

[51] P. Jensen. Calculation of rotation-vibration linestrengths for triatomic molecules using a variational approach. *J. Mol. Spectrosc.*, 132:429–457, 1988.

[52] K. J. Higgins, S. M. Freund, W. Klemperer, A. J. Apponi, and L. M. Ziurys. The rotational spectrum and dynamical structure of LIOH and LiOD: A combined laboratory and ab initio study. *J. Chem. Phys.*, 121:11715, 2004.

[53] R. J. Barber, J. Tennyson, G. J. Harris, and R. N. Tolchenov. A high accuracy computed water line list. *Mon. Not. R. Astron. Soc.*, 368, 2005.

[54] P. De Laverny, C. Abia, B. Domnguez I., Plez, O. Straniero, R. Wahlin, K. Eriksson, and Jrgensen U. G. Chemical analysis of carbon stars in the local group. *Astronomy and Astrophysics manuscript*, 446:1107–1118, 2006.

[55] J. A. Fernley, S. Miller, and J. Tennyson. *J. Mol. Spectrosc.*, 150:597–609, 1991.

[56] C. R. Le Sueur, S. Miller, and J. Tennyson. On the use of variational wavefunctions in calculating vibrational band intensities. *Mol. Phys.*, 76:1147–1156, 1992.

[57] J. R. Henderson and J. Tennyson. All the vibrational bound states of $H_3^+$. *Chem. Phys. Lett.*, 173:133–138, 1990.

[58] H. Y. Mussa and J. Tennyson. Calculation of the rotation-vibration states of water up to dissociation. *J. Chem. Phys.*, 109:10885, 1998.

[59] J. Makarewicz. Rovibrational hamiltonian of a triatomic molecule in local and collective internal coordinates. *J. Phys. B:At. Mol. Opt. Phys.*, 21:1803–1819, 1988.

[60] F Wang. *Ab initio calculations of rotovibrational states of alkali metal ions*. PhD thesis, Departmant of Chemistry, The University of Newcastle, 1994.

[61] D. W. Schwenke and H. Partridge. *J. Chem. Phys.*, 113, 2000.

[62] T. Giensen. Molecular astrophysics: The search for interstellar carbon clusters. Technical report, Physikalisches Institut Universitat Zu Koln, 2002.

[63] G. Larsson. The $C_3$ molecule: A litterature study and spectroscopic investigation in flames and on graphite. Technical report, Lund Institute of Technology, 2002.

[64] G. J Harris. *An ab initio HCN/HNC Rotational-Vibrational Line List and Opacity Function for Astronomy*. PhD thesis, Department of Physics and Astronomy University of London, 2002.

[65] M. L Abell. *Statistics with mathematica*. Academic Press, 1999.

[66] P. W. Atkins and R. S. Friedman. *Molecular Quantum Mechanics. Third Ediction*. Zanichelli, 1997.

[67] C. N. Banwell. *Fundamentals of Molecular Spectroscopy*. McGraw-hill Book Company, 1972.

[68] J. D. Graybeal. *Molecular Spectroscopy*. International editions, 1988.